A Paleosol-Derived Environmental Perspective on MIS 3 in the Central Great Plains

By

Dakota Burt

B.S. University of Wisconsin-Oshkosh

Submitted for the graduate degree program in the Department of Geography and Atmospheric Science and the Graduate Faculty of the University of Kansas in partial fulfillment of the requirements for the degree of Master of Science.

_____
William C. Johnson, Ph.D.
Chairperson

_____
Pamela L. Sullivan, Ph.D.

_____
Stephen T. Hasiotis, Ph.D.

Thesis Defense July 19, 2018

The Thesis Committee for Dakota J. Burt certifies that this is the approved version of the following thesis:

A Paleosol-Derived Environmental Perspective on MIS 3 in the Central Great Plains

_____
William C. Johnson, Ph.D.
Chairperson

Thesis Approval July 19, 2018

Abstract

The Marine Isotope Stage (MIS) 3 Gilman Canyon Formation (GCF) is a unique stratigraphic unit prevalent throughout the Central Great Plains of North America and serves as an important underutilized archive of paleoenvironmental data. This study focuses on the GCF in central Kansas where it contains two cumulic paleosols and an intervening detrital unit, which have been radiocarbon dated ~46 ka to 24 ka, a period that spans most of MIS 3. Herein, newly obtained stable isotope, elemental, enviromagnetic, phytolith, particulate charcoal, particle size, color, and observational data from the GCF are used to generate the most comprehensive look at the MIS 3 environment in the Central Great Plains to date. In the distal portion of the Central Great Plains loess plume the GCF supported a moderately active soil community dominated by C_4 grass prairies, suggesting a warm fairly dry climate prevailed during most of MIS 3.

Acknowledgements

This project would not have been possible without the collaborative effort of many researchers who provided help in the field, laboratory, and with data interpretation. I first like to thank my committee members, Pam Sullivan and Steve Hasiotis. Pam aided me in better understanding elemental data and Steve both accompanied me to my field site and taught me how to be far more diligent with field observations. I also extend thanks to Christoph Geiss for generating and helping to interpret enviromagnetic data; Kendra McLauchlan and her laboratory assistants for assistance with sedimentary charcoal lab methods; Bruce Barnett for generating stable isotope data and instruction on sampling and laboratory procedures; Steve Bozarth for counting opal phytoliths and helping with environmental interpretation; Joe Mason for assistance with particle size samples; Jim Paces for carbonate dating and interpretation; and Michelle Nelson and Tammy Rittenour for their OSL workshop and assistance with age interpretation.

I also thank the University of Kansas and the departments of Geology and Geography and Atmospheric Sciences for use of facilities and fellowships during my time as a student. Additional funding for this research was provided by a Geologic Society of America Graduate Student Research Grant and a Kollmorgen Graduate Research Scholarship from the department of Geography and Atmospheric Sciences.

I extend a special thanks to my advisors and mentors during my time as an undergraduate and graduate student, Mark Bowen and William Johnson. Without guidance from Mark, I never would have become an earth scientist, and never would have gone on to graduate school. He has been a constant force reminding me not to

sell myself short and has always been quick to offer me help. Bill has taught me an incredible amount over the last three years, both academically and in life. His experience is seemingly limitless and his knowledge base is astounding, but he still maintains his humility and is always eager to learn more. Bill's subtle instruction has helped me push myself to become a better learner and has been paramount to my success; I am truly honored to be one of his students. Without Mark and Bill, I would not be where I am today and I consider myself very fortunate to have found both of them on my academic journey and I am happy I have them to look up to.

Lastly I want to thank my family and friends. The friends I have made in my time at KU have been very supportive and have always been around when I needed them. My family has been very patient with me, and it has been hard to be far away from them, but their support and love have been essential to my success.

Table of Contents

Abstract iii

Acknowledgements iv

Table of Contents vi

1. Introduction 1

    1.1 CGP Loess Stratigraphy 2

    1.2 Variability within the CGP Loess Plume 5

2. Study Area 6

3. Materials and Methods 7

4. Results 16

5. Discussion 24

    5.1 MIS 3 in the Northern Hemisphere and North America 24

    5.2 Stratigraphic and Environmental Interpretations 28

        5.2.1 Basal Sand, Sangamon Soil, and Loveland Loess 28

        5.2.2 GCF S2 33

        5.2.3 Detrital Unit 37

        5.2.4 GCF S1 39

        5.2.5 Peoria Loess 39

6. Conclusions 40

References 41

Tables 67

Figures 69

1. Introduction

The Central Great Plains (CGP) of mid-continental North America has some of the thickest loess deposits in the world (Bettis et al., 2003; Roberts et al., 2003). Stadial periods facilitate loess accumulation, while warmer and more stable interstadial periods, associated with glacial retreat, promote pedogenesis within the surface of loess units (Muhs and Bettis, 2003; Mason et al., 2007; Johnson et al., 2007a). These loess and paleosol sequences are useful tools for tracking changing environments (Muhs et al., 1999; Bettis et al., 2003) and are well correlated to Marine Isotope Stages (MIS), which are used to track past global climate changes as represented by oxygen-isotope curves from marine sediment cores (Hovan et al., 1989; Rea, 1994).

In the CGP, loess and its intercalated paleosols serve as ubiquitous and comprehensive depositories of paleoenvironmental data for the late Quaternary (Muhs and Bettis, 2003; Markewich et al., 2011). Paleosols are particularly useful archives because rapid burial by loess preserves soils and their innate characteristics (Olson and Nettleton, 1998; Marin-Spiotta et al., 2014), which are controlled by their formative environment. Proxy data extractable from paleosols can, therefore, be used to reconstruct paleoenvironments, and by extension, paleoclimates (Ruhe et al., 1971; Kukla, 1977; Karlstrom et al., 2008; Sheldon and Tabor, 2009). Paleosols, such as the Brady Soil of the Pleistocene–Holocene transition, have yielded several multiproxy paleoenvironmental reconstructions (e.g., Johnson and Willey, 2000; Johnson et al., 2007b; Mason et al., 2008; Marin-Spiotta et al., 2014; Woodburn et al., 2017). Other equally pervasive paleosols, such

as those associated with the Late Pleistocene Gilman Canyon Formation (GCF), however, have received little attention, leaving a notable gap in regional paleoenvironmental data that was expressed by Voelker and workshop participants (2002). An exception to this is one previous multiproxy study by Johnson et al. (2007a) at the type locality of the GCF in southwestern Nebraska; however, this single record is likely not representative of the entirety of the CGP, which has immensely variable loess sedimentation rates and spans a greater climatic gradient than any other biome in North America (Collins, 1969; Fredlund and Tieszen, 1997). Their study is focused in a unique portion of the CGP that experienced extremely high loess sedimentation rates during the Late Quaternary. New GCF-based proxy data from central Kansas are presented herein to address this paleoenvironmental data void for more source-distal loess locations in the CGP and to contribute to the growing network of GCF data.

1.1 CGP Loess Stratigraphy

In the CGP there are five prevalent loess units: the pre-Illinoian loess; the Illinoian Loveland Loess; the middle-Wisconsinan GCF loess; the late-Wisconsinan Peoria Loess; and the Holocene Bignell Loess (Figure 1). Schultz and Stout (1945) and Frye et al. (1948) were among the first researchers to recognize and characterize these loess units in Nebraska and Kansas, respectively, and these loess units were officially recognized as formations in Nebraska by Reed and Dreeszen (1965). During periods of slow or negligible loess sedimentation, soils form on the surface of these loess units, thereby creating a soil sequence that facilitates

differentiation of the units (Muhs and Bettis, 2003), although soils do form within individual loess units, such as those within the Bignell Loess (e.g., Mason, 1998; Mason et al., 2003a).

Loess and paleosols of the pre-Illinoian are the least understood of these units and have previously been characterized by diagnostic paleosols, underlying ash beds such as the Lava Creek B (Izett and Wilcox, 1982; Maat and Johnson, 1996; Johnson et al., 2007a), and are correlative to the Kennard Formation (Mason et al., 2007) and the Sappa Formation (Reed and Dreeszen, 1965). Loveland Loess rests conformably above pre-Illinoian loess and paleosols (Smith, 1942) and is one of the most regionally extensive loess units, covering the CGP, as well as part of the Missouri, Mississippi, and Ohio River valleys (Ruhe, 1983; Leigh and Knox, 1994; Mason, 2001), and has been correlated to MIS 6 using thermoluminescence (TL) ages (Forman et al., 1992; Maat and Johnson, 1996; Markewich et al., 2011). During MIS 5e–4, loess deposition ceased or was greatly diminished, allowing the Sangamon Soil to form in the uppermost Loveland Loess (Smith, 1942; Muhs et al., 1999; Mason et al., 2007; Markewich et al., 2011). Overlying the Sangamon Soil is the equally extensive MIS 3 GCF, a unit typically < 4 m thick and expressing a single or multiple cumulic, organic-rich paleosols (Reed and Dreeszen, 1965; Muhs et al., 1999; Bettis et al., 2003; Johnson et al., 2007a). The GCF was deposited slowly over ~20 k years allowing for aggradational pedogenesis over much of the CGP (Jacobs and Mason, 2007; Karlstrom et al., 2008), which often results in the GCF soil welding to the underlying Sangamon Soil, especially where GCF loess is thinnest (Johnson et al., 2007a). The GCF is coeval with the Farmdale Soil in Illinois, Pisgah Formation in

Iowa, and Roxana Silt in the Mississippi and Ohio River valleys (Follmer, 1983; Bettis, 1990; Leigh and Knox, 1993; Karlstrom et al., 2008). Peoria Loess, deposited during MIS 2, overlies the GCF and is the most regionally extensive and thickest of the loess units (Figure 2). The Peoria Loess is up to 50 m thick in southwestern Nebraska and was rapidly deposited, exhibiting little to no pedogenic alteration, except upon its termination when the Brady Soil formed (Muhs et al., 1999; Bettis et al., 2003; Roberts et al., 2003). The MIS 2–1 Brady Soil is prevalent within the CGP (Mason et al., 2008), though it is often difficult or impossible to detect without the overlying MIS 1 Bignell Loess to separate it from the modern surface soil. Where Bignell Loess is thin or absent the development of modern surface soils overprints the Brady Soil (Thorp et al., 1951; Dreeszen, 1970; Johnson and Willey, 2000).

Most loess in the CGP loess plume was derived from nonglaciogenic sources, primarily the White River Group, Arikaree Group, and Pliocene silts in southwest South Dakota (Aleinikoff et al., 1998; Mason, 2001; Mason et al., 2003; Muhs et al., 2008). A model created by Bromwich et al. (2005) established that in spring, strong low pressure systems with gusty winds and very little moisture along a very powerful jet stream could have easily mobilized dust and moved it systematically to the southeast. Loess would have been repeatedly remobilized as it moved over the Nebraska Sand Hills in multiple episodes of short-term suspension, until the sediments were ultimately deposited in southern Nebraska, eastern Colorado, and Kansas (Mason, 2001).

1.2 Variability within the CGP Loess Plume

Spatial trends in the CGP loess plume have been best observed in the thickest and most pervasive of these loess units, the Peoria Loess (Bettis et al., 2003). Peoria loess depositional trends indicate that proximal to the source region—and adjacent to the Nebraska Sand Hills—loess accumulations are thickest and gradually thin towards the southeast as a result of reduced sediment load (Mason, 2001; Bettis et al., 2003; Muhs and Bettis, 2003), a pattern mirrored by other loess units in the CGP, albeit far less dramatically. Additionally, the proximal portion of the loess plume contains more sand and coarse silt, resulting in fairly large mean grain sizes. Such easily transported grains as fine silt and clay are carried farther from their source region, resulting in mean grain size reduction toward the distal end of the loess plume (Muhs and Bettis, 2003). Changes in sediment thickness and mean grain size from the proximal to the distal portion of the loess plume results in individual loess units with unique characteristics that change gradually but drastically downwind from the source region. This phenomena is well expressed by the GCF, which is an elaborate pedocomplex with multiple soils (>3 in some cases) and loess bodies in the proximal loess plume, where sedimentation is higher, and winnows into one cumulic soil with no visible GCF loess bodies in the distal portion of the loess plume, where sedimentation is greatly reduced. For example, the GCF in a proximal location, such as the Hueftle Borrow Pit (HBP) in south-central Nebraska, is about 4.5 m thick and consists of two loess bodies and two soils; whereas, a more distal location, such as the Barton County Landfill (BCL) in central Kansas (about 300 km to the southeast of the HBP), expresses a 1.5 m thick GCF soil (Figure 3). In addition

to changes in sedimentary characteristics are differing climates that generally become warmer moving southward from the proximal region. This stresses the importance of understanding the paleoenvironment for individual units both in the proximal and distal portions of the loess plume. To date there are very little data available to track environmental change moving southward from the proximal region during MIS 3.

2. Study Area

The study area is located at the Russell County Landfill (RCL) (38.95250˚N, 98.85375˚W), 8 km north of Russell, Kansas, in the central portion of the state (Figure 4). Natural land cover in this region is mixed grass prairie situated in a dry subhumid to semiarid environment, with an annual mean temperature of 19–20˚C and 600–650 mm of annual precipitation. RCL is located on the high terrace of the Saline River, currently positioned about 450 m north of the study site, and has well-expressed sections of CGP loess stratigraphy situated ~300 m downslope and 20 m below outcropping Upper Cretaceous Greenhorn Limestone (Arbogast and Johnson, 1996). This site is in the distal portion of the CGP loess plume, therefore, loess units are thin but still individually expressed. Previous paleoenvironmental research in the CGP has been largely Nebraska based (e.g., Johnson et al., 2007a; Mason et al., 2008; Woodburn et al., 2017), so this site provides juxtaposition to those and is one of the first multi-proxy studies to focus on MIS 3 in the distal loess plume.

3. Materials and Methods

Samples were collected from three prepared profiles in excavated exposures within the landfill (RLPW1, RLP1, RCPS1) and from two continuous 6- m-long cores (RLCS1 and RLCS1B) extracted with a Giddings hydraulic coring machine ~5-m upslope (south) of the main reference exposure (RLPS1). An additional ~8.5-m-long core (RLE1) was extracted from the western side of the landfill but was only used for accelerator mass spectrometry (AMS) radiocarbon dating on paleosols (Figure 4). Cores were sheathed in 5.5-cm-diameter, transparent PTEG plastic core-tube liners to prevent contamination and for stability during transportation. Individual stratigraphic units were described, photographed, and examined for trace and body fossils both in exposure and within cores at the University of Kansas Soils and Geomorphology Laboratory.

Radiocarbon samples were collected to determine the chronology of pedogenesis for the GCF soil at this site and to expand the database of GCF ages within the CGP. Fourteen samples from both core and exposure were dated using the soil organic carbon component. Samples were extracted from 2 cm below the cleaned longitudinal surface of the core, picked for roots, dried at 60˚ C, and then pulverized prior to submission to Beta Analytic, Inc. in Miami, Florida, or to the National Ocean Sciences Accelerator Mass Spectrometry Facility (NOSAMS) in Woods Hole, Massachusetts. Each laboratory removed carbonates using an HCl wash during sample preparation.

Optically stimulated luminescence (OSL) samples were used to constrain the age of the GCF soil zone by dating the sedimentary units immediately above and

below the soils. OSL samples (14) were extracted from outcrop in opaque metal tubes (4.5x15 cm), sealed with black vinyl end caps, and secured with tape. Sediment from within 30 cm surrounding each tube was collected for the estimation of dose rates and *in situ* water content. Dose rates were estimated using U, Th, Rb, and K, measured by inductively coupled plasma mass spectrometry (ICP-MS), with an added cosmic ray contribution based on burial depth (Aitken, 1998). Ten of the 14 OSL samples were selected for analysis at the Utah State University Luminescence Laboratory in Logan, Utah, and processed following methods described in Rittenour et al. (2005). Samples were opened under amber light, wet sieved using 63-125 μm for fine-grained samples, and 150-250 μm for coarser samples, washed with 10% HCl to remove carbonates, washed with NaClO to remove organics, floated in $Na_6[H_2W_{12}O_{40}]$ to remove heavy minerals in order to isolate quartz, and cleansed of remaining feldspars using HF. Using a Risø TL/OSL reader and the single aliquot regenerative dose (SAR) technique, the equivalent dose of the samples was estimated, ultimately determining when quartz grains were last exposed to light (Murray and Wintle, 2000).

Further age control was established by $^{230}Th/^{234}U$ dating of two large carbonate nodules extracted from the Loveland Loess. When carbonates precipitate, soluble materials including ^{234}U accumulate as nodules form. Over time ^{234}U will decay into ^{230}Th, which is relatively insoluble and is sequestered in precipitated carbonates, thus the abundance of ^{230}Th in the nodule is a time function (Ku et al., 1979). Two nodules from RCP1 were submitted to the Denver, Colorado, U.S.G.S. Radiogenic Isotope Laboratory where they were analyzed following the procedures

outlined in Paces et al., (2001). Nodules were cut, cleaned, and polished and samples were then collected by removing material from microtrenches ground into the nodules or from fragments of calcite removed from the void space within the nodules. Samples were then gently crushed and picked for dark grains prior to measurement on a Finnigan MAT 262 thermal ionization mass spectrometer with a secondary electron multiplier in ion-counting mode. Final ages were calculated using detritus-corrected activity ratios.

Rock magnetic analyses of soil and sediment have been used to gauge soil development and weathering within loess through magnetic grain mineralogy, size, and concentration (e.g., Feng and Johnson, 1995; Johnson et al., 2007a; Singer and Verosub, 2007; Geiss et al., 2008; Maher, 2016). Low-field magnetic susceptibility (χ), a proxy for the total abundance of magnetic minerals (Singer and Fine, 1989), was measured using a Bartington MS2B sensor, which reports values as mass-normalized SI-values, and data were corroborated using a Kappabridge KLY-4 susceptibility system. Frequency-dependent susceptibility (χ_{fd}), a measure of the abundance of ultra-fine magnetic grains that straddle the superparamagnetic (SP) – single domain (SD) boundary (~0.01 μm for magnetite), which become more abundant during soil formation due to neoformation (Maher and Thompson 1991; Geiss and Zanner, 2006; Maher, 2016), was measured at 470 Hz (χ_{lf}) and 4.7 kHz (χ_{hf}) using a Bartington MS3 susceptibility meter equipped with a MS2B dual-frequency sensor. To estimate the error of the χ_{fd} measurements, low- and high-frequency measurements were repeated five times for each sample. Data are reported as $\chi_{fd} = \chi_{lf} - \chi_{hf}$ and $\chi_{fd}(\%) = (\chi_{lf} - \chi_{hf})/ \chi_{lf} \times 100$. Anhysteretic remanent

magnetization (ARM), a parameter heavily biased to fine SD particles (Geiss et al., 2008), was acquired in maximum AF field of 100 mT and a superimposed bias field of 50 μT using a Magnon AFD300 alternating field demagnetizer. Isothermal remanent magnetization (IRM), a proxy for the abundance of all remanence-carrying grains (Machac et al., 2007), was acquired in a pulsed field of 100 mT. Saturation isothermal remnant magnetization (SIRM) was acquired in a pulsed field of 1000 mT. Samples were subjected to tree field pulses using an ASC Model IM-10-30 impulse magnetizer. To calculate hard IRM (HIRM = (SIRM + $IRM_{backfield}$)/2) and S-ratios (S = -SIRM/$IRM_{backfield}$), the samples acquired a SIRM and were subjected to backfields of -100 mT and -300 mT immediately thereafter. An S-ratio calculated with a backfield of 300 mT, dubbed S_{300}, is used herein to create a narrowed mineralogical proxy by avoiding influence from SD grains. All remnance parameters were measured using an AGICO JR-6 spinner magnetometer. Hysteresis loops were measured using a PMC MicroMag Model 3900 vibrating sample magnetometer. The maximum field for hysteresis loops was 1000 mT, which was sufficient to saturate all samples. Prior to the calculation of hysteresis parameter data (saturation magnetization M_s, saturation remanent magnetization M_r, coercive force H_c) were corrected for paramagnetic contributions by calculating the high-field slope and subtracting the paramagnetic contribution. The coercivity of remanence (H_{cr}) was determined through a series of backfield demagnetization steps.

Particle size analysis was conducted to account for weathering or particle translocation within the GCF relative to unaltered loess and to ascertain the grain size characteristics of loess and paleosols in this region relative to other parts of the

CGP. In the northwestern region of the CGP loess plume, loess is typically composed of fine sand and coarse silt; however, transitioning to the more distal part of the loess plume (to the south and southeast), grains become finer, typically fine silt and clay (Mason et al., 1994; Muhs and Bettis, 2003). With the study site being in the more distal part of the loess plume, loess was expected to have high contents of clay and/or fine silt. A total of 253 samples were collected from core (RLCS1) at 2.5 cm intervals. Following rootlet removal, samples were then soaked in 20 mL of 25% H_2O_2 for 48 hours at 60˚C to remove detrital organics (Mason et al, 2003b; Sandström et al., 2005). Samples were then decanted and sonicated in deionized water for 3 minutes prior to analysis using a Malvern Mastersizer 2000 laser diffraction particle size analyzer.

Soil color can be used to approximate melanization and rubification within soils and can be a proxy for ascertaining soil organic carbon levels (Wills et al., 2007). Both CIELAB color space and Munsell color data were derived using a Konica Minolta CM-700 handheld spectrophotometer on moist soils cores and on dried samples within 8 cm^3 plastic cubes extracted from RLCS1. CIELAB color parameters include the values L^*, a^*, and b^*, where lightness, L^*, represents the darkest black at $L^* = 0$, and the brightest white at $L^* = 100$. The color channels, a^* and b^*, indicate true neutral gray values at $a^* = 0$ and $b^* = 0$. The red/green opponent colors are represented with green at negative a^* values and red at positive a^* values, whereas the yellow/blue opponent colors are represented with blue at negative b^* values and yellow at positive b^* values. Color data were recorded at 2.5 cm intervals following white-standard calibration.

Sedimentary charcoal within soils can be used to broadly characterize fire regimes, specifically fire frequency and area burned (Daniau et al., 2010; Leys et al., 2015; Leys et al. 2017). Charcoal samples (45) were collected from core (RLCS1B) and exposure (RCPS1): 30 from the GCF and 15 from adjacent units (i.e., Sangamon Soil, detrital unit, and Peoria Loess). One cm^3 from each sample was pulverized, treated with 20 mL of 10% HCl at room temperature for 48 hours to remove carbonates and then in 20 mL of 25% H_2O_2 at room temperature for an additional 48 hours to bleach the sample and oxidize organics. A 63-µm sieve was used to remove clay particles from samples, and the remaining sediment was added incrementally to a petri dish where charcoal pieces were counted under a 20-80x (typically 40x) magnification binocular microscope with a grid underlying the petri dish to facilitate counting (Leys et al., 2017). Sedimentary charcoal fragments < 63 µm were not counted in this study because they may not have been locally derived and would not contribute to the reconstruction of local fire regimes (Clark, 1988; Clark et al., 1998; Forbes et al., 2006).

Opal phytoliths found within soils form from the precipitation of hydrated silicon dioxide ($SiO_2 \cdot nH_2O$) within plant cells, on cell walls, and between cells. Plant communities can be reconstructed based on the diagnostic shapes of the phytoliths and, hence, the climatic conditions during phytolith deposition (Wilding and Drees, 1971). Herein, diagnostic phytoliths used are Pooideae (pooids), *Stipa*-type Pooidoideae, Chloridoideae (chloridoids), Panicoideae (panicoids), and *Aristida*-type Arunidoideae (arundinoids), in addition to those from deciduous arboreal species. Phytoliths were extracted and classified for 24 samples collected from core (RLCS1)

and exposure (RLP1). Samples were washed with HCl to remove carbonates, deflocculated with $Na_4P_2O_7$ to remove organics and fine particles, centrifuged, and filtered through a 7-µm filter. Samples were then oxidized with KOH to remove remaining organics, isolated using $ZnBr_2$ heavy-liquid separation, and washed and dehydrated with butanol prior to transfer into in 1-dram vials. Phytolith isolates were mounted on standard glass microscope slides using immersion oil under cover glasses, which were sealed with nail lacquer. A minimum of 200 phytoliths were counted for each sample at 625x magnification using a petrographic microscope (Bozarth, 1993). Phytolith data can be very difficult to interpret because certain distinctive phytolith forms are produced to some degree in almost all plants, like those associated with common C_3 grasses (e.g., *Festucoid*-type Pooideae), thus, resulting in C_3 plants almost always appearing to be the dominant plant species even when they are not (Fredlund et al., 1985; Piperno, 2006), so appropriate care must be taken when interpreting any change in phytolith concentrations. To better characterize phytolith data, indices were used to show trends in the data. The phytolith woodland-grassland index established by Cordova et al. (2011) was used as a proxy to estimate the amount of wooded vegetation in the region by expressing the total number of grass phytoliths over the total number of woody plant phytoliths multiplied by 100. This index is comprised of four categories: 1) < 50 represent open grassland; 2) 50–200 express grasslands with scattered shrubs (open woodland); 3) 200–400 represent where canopy cover is ≥ 40% (closed woodland; Gonzalez et al., 2006); and 4) > 400 are closed canopy forests. Additionally, an aridity index proposed by Diester-Haass et al. (1973) was

implemented to determine relative moisture availability in this region. The index is a ratio of chloridoid phytoliths over the sum of the chloridoid and panicoid phytoliths, where a ratio close to 1 represents very dry environments that only promote the growth of short grasses, and values close to 0 are representative of moist environments with tall grasses.

Stable isotopes and organic C were used to characterize plant communities during loess deposition and soil development (Johnson et al., 2007a, b; Woodburn et al., 2017). Stable carbon isotopes ($\delta^{13}C$) from plant material differentiate plants based on whether they use the C_3 or C_4 photosynthetic pathway (O'Leary, 1981). C_3 (cool season grasses, shrubs, most trees) typically have $\delta^{13}C$ values between -32‰ and -20‰ (Ode et al., 1980), whereas C_4 plants (predominately warm season grasses) have $\delta^{13}C$ values between -17‰ and -10‰ (O'Leary, 1988). High $\delta^{13}C$ values are the result of a high contribution of C_4 grasses to soil organic C and are indicative of warm temperature regimes and/or drier conditions (Teeri and Stowe, 1978; Osmond et al., 1982) because the C_4 photosynthetic pathway is far more efficient in warmer and drier environments, providing a competitive advantage over C_3 plants (Björkman, 1971; Black, 1973; Fredlund et al., 1985). Total organic C within soils is largely related to plant productivity which is primarily a function of temperature and moisture regimes (Jobbagy and Jackson, 2000). Pairing organic C and total N values provides a C/N ratio, which not only distinguishes terrestrial and aquatic environments but also serves as a metric for relative soil activity (Stevenson and Cole, 1999; Johnson et al., 2007a). Samples (124) taken from RLCS1 were analyzed at the University of Kansas Keck Paleoenvironmental and Environmental

Stable Isotope Laboratory (KPESIL) for $\delta^{13}C$, $\delta^{15}N$, total N, and organic C. Samples were oven dried at 60˚C, pulverized, picked for roots, and decarbonated with 10 mL of 0.5 M HCl, repeated as necessary until samples were no longer reactive. Deionized water was used to bring samples back to a neutral pH, which were then dried at 60˚C, pulverized, and loaded into tin capsules. Samples were combusted at 1060˚C in a Costech Elemental Analyzer and transferred to a ThermoFinnigan MAT 253 mass spectrometer for assay, along with specified standards. After these analyses, resulting data were used to calculate the percent contribution of C_4 plants to organic carbon following a simple mixing model developed by Ludlow et al. (1976) and subsequently adopted by several researchers investigating soil and paleosol $\delta^{13}C$ signals in central North America (e.g., Nordt et al., 1994; Boutton et al., 1998; Feggestad et al., 2005; Johnson et al., 2007a; Holliday et al., 2008).

Geochemical data were obtained to track changes in soluble ions and to serve as provenance indicators (Muhs et al., 2008; Yang et al., 2017). Bulk samples (35) for geochemical analysis were taken from core: 5 individual samples from the upper 3 m of core and every 10 cm through the lowermost 3 m of core. Approximately 15 g of each sample were submitted to ALS Minerals (Reno, Nevada) for analysis, where samples were dissolved with a four-acid digestion—using HNO_3, $HClO_4$, HF, and HCl—and measured via ICP-MS for 48 elements; additional portable x-ray diffraction (pXRF) analysis was conducted for Si, Ti, and Zr due to the possibility of incomplete acid digestion.

4. Results

Core and exposure observations indicate site stratigraphy consisting of a basal alluvial sand unit overlying Cretaceous bedrock (strath terrace), Loveland Loess, Sangamon Soil, GCF consisting of two soils (GCF S2 and GCF S1) with an intervening detrital unit, and Peoria Loess at the top of the section. The overlying Brady Soil, Bignell Loess, and modern surface soil had been mechanically removed through landfill operations at most sample locations. The base of the profile from RLCS 1 contains redoxomorphic features expressed within a fine-textured alluvial sand unit, which is overlain by ~40 cm of Loveland Loess along a boundary with observable loading features. The Loveland Loess is light brownish gray in color (0.7Y 6/2) and contains large carbonate nodules (≤ 7x5 cm) precipitated from material transported downward from the overlying Sangamon Soil. The Sangamon Soil, formed in the uppermost Loveland Loess, is easily distinguished by its reddish brown coloration (9YR 5/3), subangular blocky structure, and clay skins. Such trace fossils as rhizoliths and *Naktodemasis* (adhesive meniscae backfilled burrows; Hasiotis and Dubiel, 1994; Smith et al., 2008) are present in this soil, indicating near-surface biological processes.

Overlying the Sangamon Soil is GCF S2, which is easily distinguished by its melanization relative to other units in the profile. The lowermost GCF S2 is welded to the uppermost Sangamon Soil resulting in ~10-cm-thick zone that shares characteristics from both soils, creating a transitional boundary. Above the transition zone, GCF S2 is dark greyish brown (9YR 4/2), expressing very little structure and exhibiting abundant trace fossils. *Edaphichnium* (earthworm burrows;

Bown and Kraus, 1983) and *Naktodemasis* are numerous in the soil, but rhizoliths are far more prevalent, so much so that they have created a coarse woven cloth-like pattern. In the upper 20 cm of GCF S2 *Edaphichnium* were no longer present, *Naktodemasis* frequency increased, and, while rhizoliths were still present, they were less numerous and filled with carbonates. Additionally, large cracks were observed running from the top of GCF S2 downward, in some instances up to 1 m deep and 3 cm wide, and infilled with coarse material from the overlying detrital unit. Rock fragments of local origin are embedded in the uppermost 20 cm of GCF S2, marking a transitional boundary with the detrital unit, consisting of the rock fragments mixed with silt-sized material and interpreted as slope wash. The detrital unit is ~50-cm thick and light yellowish brown (0.2Y 6/3) with no visible evidence of pedogenesis and no trace fossils except for what appear to be hoof prints of large herbivores (e.g., Kurén and Anderson, 1980; Loope, 1986). Trough crossbedding is present in lowest 20 cm of the unit, where the greatest concentration of angular clasts occurs, whereas the upper 30 cm has fewer angular rock fragments and is composed primarily of silt. Above the detrital unit is GCF S1, a relatively weakly developed brown (9.7YR 5/3) soil, with very few trace fossils except for sparse rhizoliths observed in core (covered interval in outcrop). Peoria Loess, overlying the GCF S1, is greyish brown (.4Y 5/3) and uniform through the top of the profile with no evidence of pedogenesis, structure, or trace fossils.

Throughout the entire profile, one of the most unique and consistent trace fossils were ground-dwelling rodent burrows. All cores and exposures have ground-dwelling rodent traces, which appeared in the sand unit, the Sangamon Soil, GCF S2,

and the detrital unit. Burrows were recognizable because they are infilled with sediment from contrasting overlying units. Almost all ground-dwelling rodent traces at this site have fill material from an MIS 3 unit (i.e., GCF S2, the detrital unit, and GCF S1) signifying these units served as the staging ground for these rodents.

Ten AMS ^{14}C ages were obtained in core and profile for the GCF soil (Table 1). Ages for GCF S2 limit it to between 45.6 ka and 31.6 ka, and those for the GCF S1 limit it to between 30.2 ka and 24.9 ka, though some ages were out of stratigraphic sequence. These ages are consistent with those reported in previous studies (e.g., Johnson et al., 2007a; Muhs et al., 2008; Layzell et al., 2016), which constrain the age of the GCF soil zone between 45 ka and 24 ka.

OSL ages were determined for the basal sand unit, Loveland Loess, Sangamon Soil, detrital unit, and Peoria Loess (Table 2). Ages below GCF S2 were not all in stratigraphic sequence and were anomalously young based on their stratigraphic position and previously determined IRSL and TL ages. The basal sand unit was dated using two separate samples to 51.16 ka and 54.06 ka, both of which are younger than underestimated Loveland Loess ages presented herein and are out of stratigraphic sequence; however, the similarity of these ages—both from different outcrops—make these unique outliers. At this site the Loveland Loess OSL dated to 60.50 ka, which is far younger than previous MIS 6 estimations (Forman and Pierson, 2002; Mason et al., 2007). The Sangamon Soil ages of 43.59, 48.05, and 61.34 ka appeared to be too young, although the Sangamon Soil is not yet well dated beyond correlations to the deep-sea or ice-sheet record (Curry and Pavich, 1996; Grimley et al., 2003; Markewich et al., 2011). The detrital unit was dated to 31.99 ka,

falling within the AMS ^{14}C ages for GCF S1 and GCF S2. OSL ages for the Peoria Loess were between 27.43 ka and 16.60 ka, and were in stratigraphic sequence.

Two carbonate nodules were dated using $^{230}Th/^{234}U$, returning four separate ages. These nodules exhibited vuggy porosity with numerous angular fragments, and exhibited low concentrations of ^{234}U, which is common for nonphreatic carbonates deposited by percolating water (Chung and Swart, 1990). Both carbonate nodules were used to calculate two separate ages by taking samples from different parts of both nodules. One nodule was dated to 68±27 and 65±18 ka and the other was dated to 37±16 and 58±25 ka. Large errors associated with these ages are due to very low concentrations of both ^{234}U and ^{230}Th within the samples, and the youngest nodule age (37 ka) is presumed to have underestimated the age due to calcite additions following original formation of the nodule. The U.S.G.S. Radiogenic Lab derived a mean of the oldest three age estimates weighted by their individual uncertainties to yield a more precise estimate age of 64±12 ka.

Three soils are highlighted in the profile by enviromagnetic data, particularly χ, χ_{fd}, and ARM/IRM (Figure 5). Lowest χ values are in the sand and Loveland Loess but abruptly increase into the Sangamon Soil, ultimately reaching highest sustained values in GCF S2. In the detrital unit, χ drops significantly but recovers slightly going into GCF S1 and is maintained at that level throughout the Peoria Loess. A similar pattern displayed in χ_{fd} serves to further outline soils in the profile. Loveland Loess, the detrital unit, and Peoria Loess have χ_{fd} values of ~2–2.5%, whereas the Sangamon Soil has values ~3–3.5%, GCF S2 ~5–5.5%, and GCF S1 ~4–4.5%. ARM/IRM ratios, show patterns similar to those of χ and χ_{fd} where Loveland Loess,

the detrital unit, and Peoria Loess display relatively low values while the Sangamon Soil and GCF S2 have high values, and GCF S1 has values slightly lower than the other soils. Coercivity, expressed as S_{300} (Figure 5), is low overall. The basal sand and the Loveland Loess have the lowest S_{300} values but rose rapidly in the Sangamon Soil and stayed relatively high in GCF S2, mimicking χ. Above GCF S2 coercivity increases steadily but at a gradual rate.

Particle size within the profile was predominately silt (75–90%) and only displayed minor variations among the individual stratigraphic units (Figure 6). Two segments within the profile, however, deviate from this trend, a ~1-m-thick zone spanning the uppermost GCF S2 and the detrital unit, where sand increases to ~45%, and a sand unit containing ~80% sand at the base of the profile. Clay content is consistently 10–20% throughout most of the units but is slightly lower in the Peoria Loess and drops to <1% in the basal sand. The large silt fraction was further divided into four categories (very fine silt, fine silt, medium silt, and coarse silt) to account for variations not discernable in the relatively static sand, silt, and clay classes (Figure 6). Very fine silt is the predominant grain size throughout the profile, typically 30–40% of the total silt fraction, but distinct 10–15% increases in very fine silt occur in the Sangamon soil, GCF S2, and GCF S1, at the expense of coarse and medium silts.

Spectral color tracked melanization and rubification of sediments and soils in each unit (Figure 7). L^* values are at their lightest and brightest ($L^* = 68$) at the bottom of the profile and steadily decrease through the Sangamon Soil, becoming darkest and most melanized ($L^* = 34$) in the middle of GCF S2. L^* steadily increases

upward in the detrital unit to 63 at 300–250 cm but then dips to 43 in GCF S1 and stabilizes at about 50 through the Peoria Loess. Values of *a** indicate a peak of accentuated redness within the Sangamon Soil, and *b** values show two peaks, one within the Sangamon Soil, and another in the detrital unit, where yellowish rock fragments are present.

Sedimentary charcoal fragment concentrations were somewhat limited within this stratigraphic sequence but did vary in frequency stratigraphically (Figure 8). Charcoal counts were highest in the upper part of the GCF S2, with concentrations decreasing steadily downward into the Sangamon Soil. Charcoal counts immediately above GCF S2, in the detrital unit, were among the lowest in the profile but did increase rapidly in the upper GCF S1 and lower Peoria Loess.

Phytolith assemblages highlighted unique vegetation patterns within the GCF and adjacent units (Figure 9). The lowest documented phytolith assemblage—in the middle Sangamon Soil—contains a high concentration of deciduous woody vegetation, expressed with a moderate concentration of chloridoids and panicoids. This pattern continues through the top of the Sangamon Soil where sponge spicules are also present. In the transition zone between GCF S2 and the Sangamon Soil, deciduous woody plants are still prevalent, *Stipa*-type pooids appear, panicoid presence greatly increases, and chloridoids have a very low concentration. Chloridoids were fairly prevalent throughout GCF S2, corresponding with a period where woody vegetation phytolith concentrations are low or nonexistent. GCF S2 also has four distinct periods where pooid concentrations rose, but panicoids and chloridoids were still well represented. In the uppermost GCF S2, chloridoids

decline rapidly, panicoids rise, and woody vegetation returns to a detectable level. Transitioning from GCF S2 to the detrital unit, pooids dominate, panicoids and deciduous woody vegetation are present, and sponge spicules reappear. The upper portion of the detrital unit shows a decrease in pooids and a stark decrease in phytolith concentration. In the transition between the upper detrital unit and GCF S1, chloridoids and arundinoids greatly increase, accompanied by a slight rise in *Stipa*-type pooids. Chloridoids decrease rather abruptly and are replaced by panicoids and arundinoids in the middle of GCF S1, which is also where pooids fall to their lowest concentration. The uppermost GCF S1 and adjacent Peoria Loess exhibit a decrease in deciduous woody plants and maintain a limited concentration of pooids, but have a greater prevalence of *Stipa*-type pooids and chloridoids. The phytolith woodland-grassland index indicates that the Sangamon Soil, detrital unit, and GCF S1 were developed or deposited under closed woodlands, and that GCF S2 and the Peoria Loess were deposited under open grasslands, with periodic appearance of scattered shrubs. The aridity index is highest in GCF S2, in the uppermost and lowermost GCF S1, and in the Peoria Loess, where values are close to or equal one. In contrast, there are two distinct parts of the profile where the aridity index is very low, the transition between the Sangamon Soil and GCF S2, and a zone that goes from the uppermost GCF S2 into the lower half of the detrital unit. Values of the aridity index fluctuate abruptly, with the starkest changes occurring in the transitional zone between units.

Stable carbon isotope values in the basal sand were ~-29.5‰ and increase rapidly upward through the Loveland Loess until stabilizing at ~-21‰ in the

Sangamon Soil. In the transition from the Sangamon Soil to GCF S2 and upward throughout GCF S2, values continue to increase to a maximum at ~-14‰, where they remain constant through the upper half of GCF S2. Values dip to -18‰ transitioning from GCF S2 to the detrital unit but then rebound to -14‰ in GCF S1, before dropping to <-21‰ in the Peoria Loess (Figure 10). Percent C contribution from C_4 plants mimics the same pattern as the stable carbon isotopes, reaching its maximum in GCF S2 and lowest in the loess units and basal sand.

Organic C data (Figure 10), derived in tandem with $\delta^{13}C$ data, display two distinct modes in the profile, a primary one in GCF S2 (0.91%) and secondary one in GCF S1 (0.57%). Organic carbon levels within loess units are significantly lower, and transitions between loess units and paleosols display abrupt changes in organic carbon content. Total nitrogen displayed a pattern similar to organic carbon, highlighting the soils in the profile and was closely tracked by $\delta^{15}N$ data. C/N ratios are typically higher in the paleosols and lowest in the loess; however, apart from the elevated values of GCF S2, the ratio shows minimal variation in the other units, with values ranging 5–8. Modern soils generally have C/N ratios around 10–12 (Stevenson and Cole, 1999), which corresponds well with values in GCF S2, though GCF S1 and the Sangamon Soil have lower C/N ratios (~7–8).

Previous studies indicated that the provenance of loess in the CGP is the White River Group, Arikaree Group, and Pliocene silts in southwest South Dakota (Mason, 2001; Muhs et al., 2008). Muhs et al. (2008) used derived K/Rb and Ti/Nb ratios as provenance indicators because of the propensity of the trace element Rb to substitute for K in certain minerals such as K-feldspars and micas (Heier and Adams,

1964; Lange et al., 1966), and because the trace element Nb will substitute for Ti, although this ratio is largely constrained by the presence of Ti in the source rocks, which can be variable within individual units (Parker and Fleischer, 1968). Both of these ratios can, however, display high variability in their values, due primarily to the high mobility of K and the low abundance of Ti, which makes small changes in Ti concentration account for large changes in its ratio, thus the Ti/Nb ratio is far noisier. Muhs et al. (2008) determined that the three sources collectively have K/Rb ratios between 150–250 and Ti/Nb ratios of 180–300 and used these parameters to determine the provenance for the loess and soils in the proximal portion of the CGP loess plume. These same elemental ratios were derived from the soils and loess at this distal site (Figure 11), and data are within the Muhs et al. (2008) ranges, thus affirming that loess and paleosols from both the proximal and distal portion of the CGP loess plume share a common provenance. The K/Rb ratio shows a unique pattern of K depletion near the top of GCF S2 that is accompanied by K enhancement lower in that unit, and the basal sand unit has a K/Rb ratio >250, which is the highest in the profile. The Ti/Nb ratio was noisy overall but did exhibit two periods of gradual Ti enhancement within GCF S2, and at the top of GCF S2 the Ti/Nb ratio exceed the range (>310) for the expected parent material.

5. Discussion

5.1 MIS 3 in the Northern Hemisphere and North America

MIS 3 was a period of rapidly fluctuating climates (Ahn and Brook, 2008), as reflected by multiple Dansgaard-Oeschger (D-O) events and Heinrich events

(Heinrich, 1988; Dansgaard et al., 1993). D-O events are shifts between glacial growth (stadials) and glacial retreat (interstadials) observed using $\delta^{18}O$ data from Greenland ice cores and marine sediment cores (Shackleton and Opdyke, 1973; Dansgaard et al., 1993). Several D-O events are observed in $\delta^{18}O$ data from Greenland ice core NGRIP during MIS 3 (Stuiver and Grootes, 2000), revealing several millennial-scale, abrupt temperature changes (Wang and Mysak, 2006) that result in a rapid succession of stadials and interstadials (Bond et al., 1993). As with D-O events, Bond cycles (Bond and Lotti, 1995) track changes in temperature but over longer time scales and are terminated by Heinrich events, episodes of ice discharge into the North Atlantic (Heinrich, 1988; Bond et al., 1992). Rising temperatures associated with D-O events coincide with changes in thermohaline and atmospheric circulation systems including reduced water temperatures in the Gulf of Mexico that potentially disrupt the northward flow of moisture to the interior United States (Bond et al., 1992; Grimm et al., 1993; Schmidt et al., 2006), or a northward shift of the ITCZ, which would move global high pressure systems farther into the Northern Hemisphere (Peterson and Haug, 2006).

GCF S2 and S1 development coincides with the occurrence of 10 D-O cycles, and three Heinrich events, although individual D-O events are not resolvable in the developing soil sequence (Figure 12). Though Wunsch (2006) argued that D-O events are limited to only Greenland and are product of prevailing wind fields rather than North Atlantic ocean circulation, Clark et al. (2002) closely coupled Northern Hemisphere climate to Atlantic meridional overturning circulation, and recent research including the use of a Pa/Tr tracer from North Atlantic sediments indicates

a connection between Atlantic meridional overturning circulation and the D-O events (Henry et al., 2016; Lynch-Stieglitz, 2017).

Despite the climate variability, MIS 3 is characterized by increased maximum summer insolation (Figure 12; Berger and Loutre, 1991), relatively mild temperatures (Svensson et al., 2006; Van Meerbeeck, et al., 2009), reduced atmospheric dust (Ruth et al., 2003; Újvari et al., 2017), and ice-sheet masses approximately half the size of that during LGM (Löfverström et al., 2014). Models indicate that annually global temperatures were 1.7˚C warmer during MIS 3 than the LGM and that changes of as little as 0.3˚C caused shifts between stadials and interstadials (Van Meerbeeck et al., 2009).

In central North America, very little has been done to characterize the environment during MIS 3 (Voelker and Workshop Participants, 2002). Two disparate speleothem studies focused on $\delta^{13}C$ and $\delta^{18}O$ from Crevice Cave, Missouri (Dorale et al., 1998), and Reed's Cave in the Black Hills of South Dakota (Serefiddin et al., 2004) are the first regional attempts to decipher the MIS 3 environment using relatively high resolution data. Dorale et al. (1998) suggested that 55 to 37 ka was a relatively cold time period followed by warming through 25 ka, and Serefiddin et al. (2004) reported data displaying distinct oscillating warming peaks at ~32, ~36, ~38, and ~44 ka, with intervening relatively colder temperatures. Overall, speleothem data from both of these sites are noisy but did reveal climate shifts that display some agreement with D-O events though are not well correlated to such proxies as phytolith concentrations, organic C, charcoal counts, color, or enviromagnetics. Fossil pollen from several locations exhibit a cooling trend in the

late MIS 3 environment but only cover brief time intervals. Fredlund (1995), using a fossil pollen record from Cheyenne Bottoms in central Kansas, suggested this wetland was inundated and surrounded by a mesic grassland and sage steppe from ~34 ka to ~29 ka. Grüger (1973) reported that savanna or steppe vegetation communities dominated the landscape prior to 33 ka, based on a fossil pollen record from Arrington and Muscotah marshes in northeast Kansas, which was subsequently replaced by spruce. In western Missouri, King (1973) used the fossil pollen record from Boney Springs to suggest that a pine parkland dominated the landscape prior to 31.6 ka, which was replaced by invading spruce. Several species of Mollusca, found in the uppermost GCF at multiple locations, helped to corroborate the fairly moist and cool environment of the late Wisconsinan in the region (Leonard, 1951; Frankel, 1956; Wells and Stewart, 1987; Rousseau and Kukla, 1994). Subsequently, Johnson et al. (2007a) used $\delta^{13}C$ data generated from the GCF at Buzzard's Roost, Nebraska to argue that C_4 grasses were dominant during an extended soil forming interval from ~38 ka to 30 ka, which was reflective of warm temperatures during a period of increased peak summer insolation (Berger and Loutre, 1991). Prior to 38 ka and after 30 ka plant communities shifted rapidly toward C_3 indicating cooler conditions. Overall, MIS 3 was a period of landscape stability expressed in fluvial (Johnson, 1993; Arbogast and Johnson, 1996; Sherman and Johnson, 2006; Hanson et al., 2010; McLean, 2010; Layzell et al., 2015; Mandel et al., 2016), ephemeral lake and wetland (Hofman et al., 1992; Fredlund, 1995; Jacobs et al., 2007; Baker et al., 2009; Bowen and Johnson, 2012; Bowen et al., 2018), and aeolian environments (Feng and Johnson, 1995; Pye et al., 1995; Hanson et al.

2010; Werner et al., 2011; Johnson et al., in review), followed by a period of rapid sedimentation associated with advancing ice sheets and Peoria Loess deposition.

Herein, MIS 3 is discussed in the context of the GCF, which was deposited during that time. To provide environmental context, units both above and below the GCF are included to address the environment leading into and following MIS 3. The stratigraphy at this site is reflective of a fairly typical section in the CGP loess plume, as it contains loess bodies and intercalated paleosols observed throughout the CGP (Frye and Leonard, 1951; Reed and Dreeszen, 1965). Stratigraphy at this site contains a basal sand unit not common throughout the CGP, Loveland Loess capped by the Sangamon Soil (~MIS 6–4), two GCF soils with an intervening detrital unit from local slopes (MIS 3), and Peoria Loess (MIS 2) caps the section.

5.2 Stratigraphic and Environmental Interpretations

5.2.1 Basal sand, Loveland Loess, and Sangamon Soil

Disregarding the young OSL ages, the basal fluvial sand unit was presumably deposited during late MIS 6 or early MIS 5 by the Saline River, presently 15 m below the unit and 450 m to the north of the site. Further, the sand does not share the same provenance as the overlying loess units and soils because the Saline River drainage basin is entirely within the Cretaceous bedrock landscape of central Kansas and as a result has a K/Rb ratio much higher than the overlying units. Though the OSL ages of 51.16 ka and 54.06 ka are nearly equivalent despite being collected from separate exposures, they are probably not accurate age indicators of the unit. Quartz grains in the basal sand most likely have anomalously weak

luminescence due to a lack of reworking and bleaching to create sufficient luminescence traps (Munyikwa et al., 2011; Demuro et al., 2013); also, ages may have been reduced by grain bleaching and reworking via bioturbation (Halfen and Hasiotis, 2010a , b; Hanson et al., 2015), or water content of the sample may have been underestimated, thereby not accounting for dose rate attenuation. Generally, the basal sand unit contains very little magnetic material, as reflected in the low χ_{fd}, ARM/IRM, and S_{300} values, although isolated zones of heavy redoxification cause χ to rise dramatically in specific samples (e.g., Figure 5). S_{300} values are generally low throughout the entire profile as a result of consistent maghemite to hematite ratios (Hunt et al., 1995). Thus, increases in χ and χ_{fd} reflect concurrent increases in maghemite and hematite most likely associated with more frequent wetting followed by intense dry periods.

The Loveland Loess, lowest of the aeolian loess units in this profile, is only about 50-cm thick at this site, and sits conformably at the bottom of the typical CGP loess stratigraphy seen at this site and regionally. This unit and all overlying units share K/Rb and Ti/Nb ratios indicating their provenance is the White River Group, Arikaree Groups, or Pliocene Silts (Aleinikoff et al., 1998; Mason, 2001; Muhs et al., 2008) and that the sediment grains were likely repeatedly reworked and mobilized by short-term suspension prior to deposition at the study site (Mason, 2001; Muhs et al., 2008). Loveland Loess has previously been TL dated 110–165 ka (Forman et al., 1992; Maat and Johnson, 1996; Mason et al., 2007), which is consistent with MIS data but about 90 k yrs older than OSL ages reported herein. This age disparity may be attributable to underestimated water content or bioturbation, but, unlike the

basal sand, this unit has been repeatedly bleached and reworked during transport so dim grains are less likely the cause for underestimation. Dim sand grains from the underlying sand, however, may have been mixed in with the loess during deposition, as observed in the elevated sand content in this unit relative to the overlying paleosols and Peoria Loess.

Cool season C_3 plants dominated the early Loveland Loess environment but rapidly transitioned to a mixed C_3 and C_4 plant community during latter Loveland Loess deposition. The shift towards C_4 plants indicates a warming trend seemingly accompanied by a more biologically active surface reflected in all magnetic parameters, organic C, and N increasing in the upper Loveland Loess. Furthermore, $\delta^{13}C$, organic C, and N values derived from the top of the Loveland Loess are similar to those from the Sangamon Soil. Carbonates, among other constituents, were translocated downward and deposited in the Loveland Loess creating large carbonate nodules.

The Sangamon Soil formed in the uppermost Loveland Loess during a period of little to no sediment influx (Mason et al., 2007) and is the oldest soil in this profile. This unit is very easily distinguished by its reddish color, and, because of this and other field attributes, it was originally considered the B horizon for the overlying GCF soil (Swineford and Frye, 1951; Thorp et al., 1951). Due to presumed antiquity and lack of organic C, OSL was used to date the soil; however, OSL dating soils introduces its own problems including changing dose rates over time as minerals transform and translocation of material (Aitken, 1998). The oldest Sangamon Soil OSL age reported herein (61.34 ka) is consistent with a previous TL

age reported by Feng et al. (1994) at the BCL but is at least 40 ka younger than the other TL ages, including 122 ka from Markewich et al. (2011) at Phillips Bayou in Arkansas and 103 ka from Muhs (unpublished data) at the BCL. The younger two OSL ages from this study (43.59 ka and 48.05 ka) are currently the youngest reported Sangamon ages and are stratigraphically in sequence but do fall short of the MIS 5e estimations (Curry and Pavich, 1996; Bettis et al., 2003; Johnson et al., 2007a; Markewich et al., 2011). Further age control needs to be established for the Sangamon Soil to understand the age constraints of this unit.

Previous researchers deduced that in the Mississippi Valley, the Sangamon Soil formed under conditions warmer and wetter than present (Muhs and Bettis, 2003) or under warm to hot conditions with alternating seasonal or decadal wet to dry intervals (Markewich et al., 2011). In southwestern Nebraska, Fredlund et al. (1985) concluded the paleosol the Sangamon Soil formed under warm and dry conditions. At this site in central Kansas, where virtually no records on the formative environment for the Sangamon Soil exist, the development of the Sangamon Soil marks a transition towards warmer and moister climates. The dominant vegetation during Sangamon development was mixed C_3 and C_4 parkland to closed canopy forest, although closed woodland was most prevalent, with some C_3 grasses (pooids), deciduous woody plants, tall C_4 grasses (panicoids), and short C_4 grasses (chloridoids). Given the prevalence of tall grasses and deciduous arboreal species, the climate was seemingly moist during Sangamon Soil development, though this site may have been in a riparian zone at that time as indicated by sponge spicules recovered from the Sangamon Soil that suggest the Saline River was either

nearby during soil development, inundating the soil, or that the sponge spicules were carried a short distance by the wind (Cordova et al., 2011). Pedogenic carbonate nodules, forming a zone in the Loveland Loess, were $^{230}Th/^{234}U$ dated and returned ages consistent with an OSL age from the Sangamon Soil at the site, suggesting water moving through the system was sufficient to translocate carbonates from the Sangamon Soil downward into the Loveland Loess. Given that the Sangamon Soil is relatively well developed, organic C and C/N ratios are low, likely due to diagenetic degradation of the soil organic matter (Salomé et al., 2010) and possible truncation of the soil surface prior to burial (Olson and Nettleton, 1998). Low particulate charcoal counts suggest there were not spatially extensive or frequent fires in this area which may be attributable to low fuel loads but is more likely reflective of a less flammable environment due to sufficiently high moisture availability (van der Werf et al., 2008; Higura et al., 2009).

The Sangamon Soil shows distinct magnetic enhancement, which is common in pedogenically modified material (Heller and Liu, 1986; Maher and Thompson, 1991; Maher, 1998, 2011). Increasing χ and χ_{fd} in this unit stems from small concentrations of neoformed SP or pseudo-single domain (PSD) magnetite and/or maghemite (Cornell and Schwertmann, 2003) which are strongly magnetic and common in soils (Geiss and Zanner, 2006; Torrent et al., 2006; Orgeria et al., 2011) and are created as a result of repeated periods of wetting and drying, particularly during the drying phase (Le Borgne, 1955; Taylor et al., 1987; Maher, 2011). The Sangamon Soil is also rich in hematite, contributing to its reddish hue, which is a weakly magnetic and contributes very little to χ and χ_{fd} (Mullins, 1977) and

accumulates in soils with prolonged warm and dry periods (Claquin et al., 1999). Increased ARM/IRM in the Sangamon Soil, also observed in GCF S2, signals that most of the magnetic material in this soil is composed of SD grains, indicative of pedogenic enhancement (Evans and Heller, 1994; Maher, 2011). As this pattern is not mirrored in χ and χ_{fd}, SP grains were likely oxidized ultimately becoming less effective magnetically possibly due to the age of this unit and how long it was exposed at the surface (Torrent et al., 2006). These magnetic parameters affirm that this soil dominated the surface for a long time and suggest that, while the environment may still have been moist, it probably experienced frequent periods of dryness (i.e., dry seasons or periodic drought).

5.2.2 GCF S2

GCF soil 2 represents a unique time period in the CGP, when aeolian sediment accumulation and pedogenesis converged to create a thick cumulic soil pedocomplex over ~15k years during MIS 3. Sedimentation in this unit was very slow, ~0.1 mm annually, and is more likely to have occurred episodically, rather than continuously, but at a sufficiently slow rate for pedogenesis to keep pace. AMS ^{14}C ages from this study are consistent with previously established ages within the GCF (Maat and Johnson, 1996; Muhs et al., 1999; Johnson et al., 2007; Layzell et al., 2015), and the ages herein are some of the oldest reported ages for this unit. A lack of complete stratigraphic agreement among the ages is attributed to the prevalence of bioturbation in this unit (Hasiotis and Platt, 2012), a characteristic of the GCF

(Schultz, 1934; Tobin 2004a, b), and perhaps to younger organic C from deep-running root networks being incorporated into the soil.

GCF S2 shares the same provenance as the Sangamon Soil, but unlike the latter does show an unusual Ti enhancement in the upper 20 cm of the soil that lies outside of the typical provenance. This same Ti enhancement was also observed in data presented in Muhs et al. (2008) and reflects the variability of Ti in the parent material, alteration during transport, or perhaps is representative of local material mixed in with the uppermost GCF S2.

GCF S2 is dominated by C_4 grasses, where they compose between 61% and 99% of the organic C and are at their highest concentration in the upper meter of this unit. The surface of this aggrading soil was occupied by prairie with occasional sparse shrubs dominated by C_4 grasses such as chloroidoids and panicoids. While both grasses favor warm environments, they prefer different moisture regimes, short-grass chloridoids prefer dry environments, like those of modern southwestern Great Plains (Fredlund and Tierszen, 1997), whereas tall grass panicoids prefer moist environments, like those in the eastern Great Plains (Fredlund and Tierszen, 1997). Dominance of chloridoids over panacoids, lack of arboreal species, and high aridity index values indicate a warm and dry environment, suggesting that during GCF S2 development the environment was semiarid to subhumid and the landscape was dominated by short grass prairie (Piperno, 2006; Cordova et al., 2011). Oddly, the surface of this soil (~310 cm) is devoid of chloridoids despite other proxies indicating it is the driest part of the unit. The surface of GCF S2 is the only part of the soil with carbonate-coated rhizoliths, no phytoliths from deciduous arboreal

species, large desiccation cracks, and the maximum of particulate charcoal counts – all of which can be coupled with at least periodic aridity. If frequent fires eliminate arboreal species, charcoal counts would rise even if the environment was moist, and, if the carbonate coated rhizoliths are the termination of a root zone from an upper unit, then the uppermost GCF S2 was likely not as arid as it initially appears, which calls into question how the surface of GCF S2 can exhibit $\delta^{13}C$ values that indicate heavy C_4 dominance with a very small presence of C_4 plant phytoliths in the soil. These plants would have been present but not producing measurable phytoliths or deeply rooted C_4 plants from overlying units continued to contribute organic C to previously buried units. The probable explanation is that GCF S2 formed under a semiarid environment and that rapid climate change terminated pedogenesis and altered the uppermost 20 cm of GCF S2 following or during burial.

GCF S2 had the most active soil community in this profile with organic C, N, and C/N ratio values reaching their maxima in conjunction with floral and faunal trace fossils displaying their greatest abundance. Rhizoliths were extremely abundant in this unit, due to the apparent deep-rooting, dense grassland community. Beetle and ground-dwelling rodent (e.g., prairie dog) traces indicate that climate was semiarid, given that most species of scarab beetles cannot reproduce in soil environments with soil moisture levels above 27% (Davidson and Roberts, 1968), and prairie dogs favor arid to semiarid short grass environments, ultimately avoiding tall grass and trees (Hygnstrom and Virchow, 1994; Virchow and Hygnstrom, 2002). Rock magnetic data further corroborate the activity of this soil by displaying strong pedogenic magnetic enhancement. GCF S2 contained the

highest concentration of neoformed SP magnetic particles, specifically magnetite and/or maghemite, but also contained a moderate concentration of high coercivity minerals such as hematite. The prevalence of maghemite and/or magnetite greatly increased χ and χ_{fd}, and an increased concentration of hematite would have maintained the S_{300} and ARM/IRM ratios, keeping values consistent with those seen in the Sangamon Soil, which ultimately suggests that GCF S2 experienced longer periods of dryness than the Sangamon Soil (Torrent et al., 2006). In previous studies, magnetic enhancement has been employed as a proxy for precipitation in the Great Plains (e.g., Geiss and Zanner, 2007; Geiss et al., 2008) and was well correlated specifically with ARM enhancement. Accordingly, ARM enhancement data from GCF S2 were plotted in accordance with the regression line established by Geiss and Zanner (2007), and, using this previously established relationship, mean annual precipitation was in the range of 500–600 mm/yr, which is slightly lower than the current mean annual precipitation in Russell, Kansas, and is consistent with the other proxies.

Some data trends in GCF S2 suggest that a large amount of water was moving through this unit, particularly when this unit was no longer aggrading. Very fine silt was highest near the base of GCF S2, suggesting that the soil was most actively weathering at the base of the unit; however, that contradicts organic C, N, and magnetic data that depict the upper and middle portion of the soil as the most active. It is more likely that water flushing through the unit translocated very fine silt downward through the profile, which would also explain why it appears there was little to no apparent weathering in the upper portion of the unit. This pattern

was not mirrored in clay, however, which is fairly uniform throughout and only increases slightly at the bottom of the soil, suggesting there was no intense weathering within this soil or this profile. A similar downward translocation trend can be seen in the K/Rb ratio: in the upper portion of GCF S2, K is depleted relative to the rest of the profile, and the lower part of the unit is K enriched, indicating a possible translocation of K within the unit. Additionally, Ca is almost completely leached out of GCF S2, which is atypical of a grassland soil in a semiarid environment. Water flushing through this unit could have easily mobilized K and Ca and could cause small grains to move downward. The detrital unit overlying GCF S2 was waterlain, and translocation probably occurred concurrently with short periods of intense overland flow associated with the detrital unit's deposition. This same pattern of strong leaching was also observed in the GCF by Feng et al. (1994) at the BCL ~80 km south of this study location, displaying a regional component to this pattern.

5.2.3 Detrital unit

The detrital unit is a locally derived slope wash unit consisting primarily of silt and angular clasts with cross trough stratification in its lower portion. The entire unit contains small rock fragments, which are likely derived from Greenhorn Limestone exposed 300 m upslope to the north of the study site and are concentrated in the lowermost ~20 cm of the unit. This unit represents a brief period of heavy sedimentation that interrupted pedogenesis during MIS 3, with OSL dating placing it between AMS ages from GCF S2 and GCF S1. The uppermost portion

of GCF S2 contains some clasts from the detrital unit indicating pedogenesis was able to keep pace with this sedimentation briefly before being rapidly buried. Provenance indicators suggest this material has the same parent as the loess and paleosols in this profile, so the loess present in the detrital unit is likely what GCF S2 was forming in but concentrated on a toe slope by water. Intense rain could have mobilized enough material to create this unit; however, deposition was probably episodic, not instantaneous.

This unit shows little to no alteration reflected in low organic C, N, C/N, and pedogenic magnetic enhancement. Plants still were predominately C_4, but they were not as prevalent as they were previously; this could be the result of increased soil moisture making conditions favorable for C_3 plants and/or sedimentation making a favorable environment for colonizing plants including pooids. Presence of sponge spicules in this unit suggests that this detrital zone experienced periods of inundation, which corroborates that this unit is waterlain. Phytolith assemblages show that the rocky lower portion of this unit was dominated by pooids with a small amount of panicoids and that the loessic upper portion of the unit had a much more dynamic plant community consisting of *Stipa*-type pooids, chloridoids, panicoids, and arundinoids. Except for the panicoids (which only make up a very small portion), these varied grasses indicate that the environment was relatively dry, creating a stark contrast between the upper and lower portion of this detrital unit, with rapidly increasing aridity upward. Low particulate charcoal counts imply rapid sedimentation, low fuel loads, and increased moisture which greatly reduced flammability.

5.2.4 GCF S1

GCF S1 marks the return of cumulic soil formation resulting from slow and steady loess accumulation over ~5 k years. This soil is best developed in the middle, with retarded development of the lowermost and uppermost portions likely due to the inhibiting effect of an increased rate of loess deposition. Organic C, N, χ, χ_{fd}, and weathering within the silt fraction all indicate a return to an active soil community. This soil is not as well developed as GCF S2 as reflected by a very low C/N ratio and decreased values of enviromagnetic parameters, organic C, and N. GCF S1 was dominated by C_4 plants like chloridoids, panicoids, and arundinoids, with the uppermost and lowermost portion of the soil being dominated by a semi-arid, short grass parkland or savanna and the middle of the unit showing prevalence of mixed tall and short grass prairie. This temporal pattern suggests that the periods of aridity led to weaker soil development at the top and the bottom of the unit and that an intervening period of increased precipitation facilitated greater mid-soil development.

5.2.5 Peoria Loess

Truncation by heavy excavating equipment removed the Brady Soil, Bignell Loess and modern surface soil, as well as the upper ~15 cm of Peoria Loess from RLCS1, leaving the remaining Peoria Loess as the only unit overlying GCF S1 at most sampling locations. Peoria Loess rapidly buried GCF S1 and marks the return of colder climates associated with the transition into MIS 2. This unit was deposited between ~27 ka and 14 ka (Bettis et al., 2003; Roberts et al., 2003; Muhs et al.,

2013), and those ages are consistent with OSL ages presented herein. Rapid loess deposition outpaced pedogenesis, resulting in little to no alteration of the parent material. Colder temperatures initiated the transition back to C_3 grasses, although phytolith data from the lowermost Peoria Loess show that initially this unit was being deposited in a warm and dry environment, probably due to the site's distal location and lower latitude. The warm and dry lowermost Peoria was a favorable environment for fires and seemingly led to extensive areas burning.

6. Conclusions

This study is one of the first high-resolution, multiproxy paleoenvironmental reconstructions of the MIS 3 environment in the distal portion of the CGP loess plume from the last glacial period. Using the GCF soils and intervening detrital unit it was determined that conditions were highly variable throughout MIS 3 in central Kansas. GCF S2, which developed from 45 ka to 32 ka, formed under warm and dry conditions that resulted in slow weathering and sufficiently slow sedimentation to facilitate aggradational pedogenesis. This semiarid prairie environment changed drastically around 32 ka, when the climate abruptly became far moister, resulting in heavy sedimentation that interrupted pedogenesis at this site and created the detrital unit. A rapid shift back to drier conditions allowed pedogenesis to resume around 30 ka resulting in the formation of GCF S1. Pedogenesis kept pace with sedimentation under a warm and somewhat moist mixed grass parkland before MIS 2 began and Peoria Loess buried GCF S1.

During MIS 3 central Kansas was warmer and receiving less sediment than the proximal area of the loess plume in southwestern Nebraska. The warmest period in the CGP corresponded with a period of increased insolation and the most extensive episode of pedogenesis in the region. Reduced sedimentation led to the GCF only containing two soils at this study site, and only one soil at sites farther south. In contrast, the GCF in sites more proximal to the source region contain two or more soils and had rapid enough deposition for loess accumulation to outpace pedogenesis, creating intervening loess bodies.

References

Ahn, J., & Brook, E. J. (2008). Atmospheric CO2 and Climate on Millennial Time Scales During the Last Glacial Period. *Science*, *322*(5898), 83–85. https://doi.org/10.1126/science.1160832

Aitken, M. J. (1998). *Introduction to Optical Dating: The Dating of Quaternary Sediments by the Use of Photon-stimulated Luminescence*. Clarendon Press.

Aleinikoff, J., Muhs, D., & Fanning, C. (1998). Isotopic evidence for the sources of late Wisconsin (Peoria) loess, Colorado and Nebraska: Implications for paleoclimate. *Dust Aerosols, Loess Soils and Global Change*, 124–127.

Arbogast, A. F., & Johnson, W. C. (1996). Surficial Geology and Stratigraphy of Russell County, Kansas. Kansas Geological Survey.

Baker, R. G., Bettis, E. A., Mandel, R. D., Dorale, J. A., & Fredlund, G. G. (2009). Mid-Wisconsinan environments on the eastern Great Plains. *Quaternary Science Reviews*, *28*(9), 873–889. https://doi.org/10.1016/j.quascirev.2008.12.021

Berger, A., & Loutre, M. F. (1991). Insolation values for the climate of the last 10 million years. *Quaternary Science Reviews*, *10*(4), 297–317. https://doi.org/10.1016/0277-3791(91)90033-Q

Bettis, E. (1990). Holocene alluvial stratigraphy and selected aspects of the Quaternary history of western Iowa. *Midwest Friends of the Pleistocene. Annual Meeting*, 1–72.

Bettis III, E. A., Muhs, D. R., Roberts, H. M., & Wintle, A. G. (2003). Last Glacial loess in the conterminous USA. *Quaternary Science Reviews*, *22*(18), 1907–1946. https://doi.org/10.1016/S0277-3791(03)00169-0

Björkman, O. (1971). Comparative photosynthetic CO2 exchange in higher plants. *Comparative Photosynthetic CO2 Exchange in Higher Plants.*, 18–32.

Black, C. C. (1973). Photosynthetic Carbon Fixation in Relation to Net CO2 Uptake. *Annual Review of Plant Physiology*, *24*(1), 253–286. https://doi.org/10.1146/annurev.pp.24.060173.001345

Bond, G., Broecker, W., Johnsen, S., McManus, J., Labeyrie, L., Jouzel, J., & Bonani, G. (1993). Correlations between climate records from North Atlantic sediments and Greenland ice. *Nature*, *365*(6442), 143–147. https://doi.org/10.1038/365143a0

Bond, G. C., & Lotti, R. (1995). Iceberg Discharges into the North Atlantic on Millennial Time Scales During the Last Glaciation. *Science*, *267*(5200), 1005–1010. https://doi.org/10.1126/science.267.5200.1005

Bond, G., Heinrich, H., Broecker, W., Labeyrie, L., McManus, J., Andrews, J., … Ivy, S. (1992). Evidence for massive discharges of icebergs into the North Atlantic

ocean during the last glacial period. *Nature*, *360*(6401), 245–249. https://doi.org/10.1038/360245a0

Boutton, T. W., Archer, S. R., Midwood, A. J., Zitzer, S. F., & Bol, R. (1998). δ13C values of soil organic carbon and their use in documenting vegetation change in a subtropical savanna ecosystem. *Geoderma*, *82*(1), 5–41. https://doi.org/10.1016/S0016-7061(97)00095-5

Bowen, M. W., & Johnson, W. C. (2012). Late Quaternary environmental reconstructions of playa-lunette system evolution on the central High Plains of Kansas, United States. *Geological Society of America Bulletin*, *124*, 146–161. https://doi.org/10.1130/b30382.1

Bowen, M. W., Johnson, W. C., & King, D. A. (2018). Spatial distribution and geomorphology of lunette dunes on the High Plains of Western Kansas: implications for geoarchaeological and paleoenvironmental research. *Physical Geography*, *39*(1), 21–37. https://doi.org/10.1080/02723646.2017.1319683

Bown, T. M., & Kraus, M. J. (1983). Ichnofossils of the alluvial Willwood Formation (lower Eocene), Bighorn Basin, northwest Wyoming, U.S.A. *Palaeogeography, Palaeoclimatology, Palaeoecology*, *43*(1), 95–128. https://doi.org/10.1016/0031-0182(83)90050-0

Bozarth, S. R. (1993). Opal phytolith analysis of shell middens at Sites P-309B and P-313N. *Prehistoric Human Ecology on the Golfo Dulce, Southwestern Costa Rica.*

Bromwich, D. H., Toracinta, E. R., Oglesby, R. J., Fastook, J. L., & Hughes, T. J. (2005). LGM Summer Climate on the Southern Margin of the Laurentide Ice Sheet:

Wet or Dry? *Journal of Climate*, *18*(16), 3317–3338. https://doi.org/10.1175/JCLI3480.1

Chung, G. S., & Swart, P. K. (1990). The Concentration of Uranium in Freshwater Vadose and Phreatic Cements in a Holocene Ooid Cay: A Method of Identifying Ancient Water Tables. *Journal of Sedimentary Research*, *60*(5). Retrieved from http://archives.datapages.com/data/sepm/journals/v59-62/data/060/060005/0735.htm

Claquin, T., Schulz, M., & Balkanski, Y. J. (1999). Modeling the mineralogy of atmospheric dust sources. *Journal of Geophysical Research: Atmospheres*, *104*(D18), 22243–22256.

Clark, J. S. (1988). Particle Motion and the Theory of Charcoal Analysis: Source Area, Transport, Deposition, and Sampling. *Quaternary Research*, *30*(1), 67–80. https://doi.org/10.1016/0033-5894(88)90088-9

Clark, J. S., Lynch, J., Stocks, B. J., & Goldammer, J. G. (1998). *Relationship between charcoal particles in air and sediments in west-central Siberia. The Holocene 8*.

Clark, P. U., Pisias, N. G., Stocker, T. F., & Weaver, A. J. (2002). The role of the thermohaline circulation in abrupt climate change. *Nature*, *415*(6874), 863–869. https://doi.org/10.1038/415863a

Collins, D. D. (1969). Macroclimate and the Grassland Ecosystem. In *The grassland ecosystem: A preliminary synthesis* (pp. 29–39). Fort Collins, CO: Range Science Department.

Cordova, C. E., Johnson, W. C., Mandel, R. D., & Palmer, M. W. (2011). Late Quaternary environmental change inferred from phytoliths and other soil-related

proxies: Case studies from the central and southern Great Plains, USA. *CATENA*, *85*(2), 87–108. https://doi.org/10.1016/j.catena.2010.08.015

Cornell, R. M., & Schwertmann, U. (2003). *The Iron Oxides: Structure, Properties, Reactions, Occurrences and Uses*. John Wiley & Sons.

Curry, B. B., & Pavich, M. J. (1996). Absence of Glaciation in Illinois during Marine Isotope Stages 3 through 5. *Quaternary Research*, *46*(1), 19–26. https://doi.org/10.1006/qres.1996.0040

Daniau, A.L., Harrison, S. P., & Bartlein, P. J. (2010). Fire regimes during the Last Glacial. *Quaternary Science Reviews*, *29*(21), 2918–2930. https://doi.org/10.1016/j.quascirev.2009.11.008

Dansgaard, W., Johnsen, S. J., Clausen, H. B., Dahl-Jensen, D., Gundestrup, N. S., Hammer, C. U., Hvidberg, C. S., Steffensen, J. P., Sveinbjörnsdottir, A. E., Jouzel, J., Bond, G. (1993). Evidence for general instability of past climate from a 250-kyr ice-core record. *Nature*, *364*(6434), 218–220. https://doi.org/10.1038/364218a0

Davidson, R. L., & Roberts, R. J. (1968). Influence of Plants, Manure and Soil Moisture on Survival and Liveweight Gain of Two Scarabaeid Larvae. *Entomologia Experimentalis et Applicata*, *11*(3), 305–314. https://doi.org/10.1111/j.1570-7458.1968.tb02059.x

Demuro, M., Arnold, L. J., Froese, D. G., & Roberts, R. G. (2013). OSL dating of loess deposits bracketing Sheep Creek tephra beds, northwest Canada: Dim and problematic single-grain OSL characteristics and their effect on multi-grain

age estimates. *Quaternary Geochronology*, *15*, 67–87. https://doi.org/10.1016/j.quageo.2012.11.003

Diester-Haass, L., Schrader, H. J., & Thiede, J. (1973). Sedimentological and paleoclimatological investigations of two pelagic ooze cores off Cape Barbas, North-West Africa. *Meteor Forshungergebnisse*, *16*, 19–66.

Dorale, J. A., Edwards, R. L., Ito, E., & Gonzalez, L. A. (1998). Climate and vegetation history of the midcontinent from 75 to 25 ka: A speleothem record from Crevice Cave, Missouri, USA. *Science*, *282*, 1871–1874.

Dreeszen, V. H. (1970). *The stratigraphic framework of Pleistocene glacial and periglacial deposits in the Central Plains*. Lawrence, Kan.: University Press of Kansas.

Evans, M. E., & Heller, F. (1994). Magnetic Enhancement and Palaeoclimate: Study of A Loess/Palaeosol Couplet Across the Loess Plateau of China. *Geophysical Journal International*, *117*(1), 257–264. https://doi.org/10.1111/j.1365-246X.1994.tb03316.x

Feggestad, A. J., Jacobs, P. M., Miao, X. D., & Mason, J. A. (2005). Stable Carbon Isotope Record of Holocene Environmental Change in the Central Great Plains, USA. *Physical Geography*, 15, 249-261

Feng, Z. D., & Johnson, W. C. (1995). Factors affecting the magnetic susceptibility of a loess-soil sequence, Barton County, Kansas, USA. *CATENA*, *24*(1), 25–37. https://doi.org/10.1016/0341-8162(94)00031-9

Feng, Z. D., Johnson, W. C., Sprowl, D. R., & Lu, Y. (1994). Loess accumulation and soil formation in central Kansas, United States, during the past 400,000 years. *Earth Surface Processes and Landforms*, *19*, 55–67.

Follmer, L. R. (1983). Sangamon and Wisconsinan pedogenesis in the midwestern United States. *Late-Quaternary Environments of the United States*, *1*, 138–144.

Forbes, M. S., Raison, R. J., & Skjemstad, J. O. (2006). Formation, transformation and transport of black carbon (charcoal) in terrestrial and aquatic ecosystems. *Science of The Total Environment*, *370*(1), 190–206. https://doi.org/10.1016/j.scitotenv.2006.06.007

Forman, S.L., Bettis, E. A., Kemmis, T., & Miller, B. B. (1992). Chronologic evidence for multiple periods of loess deposition during the late Pleistocene in the Missouri and Mississippi River Valleys, U.S.: Implications for the activity of the Laurentide Ice sheet. *Palaeogeography, Palaeoclimatology, Palaeoecology*, *93*, 71–83.

Forman, S. L., & Pierson, J. (2002). Late Pleistocene luminescence chronology of loess deposition in the Missouri and Mississippi river valleys, United States. *Palaeogeography, Palaeoclimatology, Palaeoecology*, *186*, 25–46.

Frankel, L. (1956). Pleistocene Geology and Paleoecology of parts of Nebraska and Adjacent Areas. *ETD Collection for University of Nebraska - Lincoln*, 1–391.

Fredlund, G. G. (1995). Late Quaternary Pollen Record from Cheyenne Bottoms, Kansas. *Quaternary Research*, *43*, 67–79.

Fredlund, G. G., Johnson, W. C., & Dort Jr, W. (1985). A preliminary analysis of opal phytoliths from the Eustis ash pit, Frontier County, Nebraska. In *Institute for Tertiary-Quaternary Studies-TER-QUA Symposium series*. *1,* 147–162.

Fredlund, G. G., & Tieszen, L. T. (1994). Modern phytolith assemblages from the North American Great Plains. *Journal of Biogeography*, *21*, 321–335.

Fredlund, G. G., & Tieszen, L. T. (1997). Calibrating grass phytolith assemblages in climatic terms: Application to late Pleistocene assemblages from Kansas and Nebraska. *Palaeogeography, Palaeoclimatology, Palaeoecology*, *136*, 199–211.

Frye, J. C., & Leonard, A. B. (1951). Stratigraphy of the Late Pleistocene Loesses of Kansas. *Journal of Geology*, *59*, 287–305.

Frye, J. C., Swineford, A., & Leonard, A. B. (1948). Correlation of Pleistocene Deposits of the Central Great Plains with the Glacial Section. *The Journal of Geology*, *56*(6), 501–525. https://doi.org/10.1086/625558

Galbraith, R. F., & Roberts, R. G. (2012). Statistical aspects of equivalent dose and error calculation and display in OSL dating: An overview and some recommendations. *Quaternary Geochronology*, *11*, 1–27. https://doi.org/10.1016/j.quageo.2012.04.020

Geiss, C. E., Egli, R., & Zanner, C. W. (2008). Direct estimates of pedogenic magnetite as a tool to reconstruct past climates from buried soils. *Journal of Geophysical Research-Solid Earth*, *113*. https://doi.org/10.1029/2008jb005669

Geiss, C. E., & Zanner, C. W. (2007). Sediment magnetic signature of climate in modern loessic soils from the Great Plains. *Quaternary International*, *162*, 97–110. https://doi.org/10.1016/j.quaint.2006.10.035

Geiss, C. E., & Zanner, C. W. (2006). How abundant is pedogenic magnetite? Abundance and grain size estimates for loessic soils based on rock magnetic analyses. *Journal of Geophysical Research: Solid Earth*, *111*(12). https://doi.org/10.1029/2006JB004564

Gonzalez, P., Hassan, R., Lakyda, P., McCallum, I., Nilsson, S., Pulhin, J., van Rosenburg, B., Scholes, B. (2006). Chapter 21 Forest and Woodland Systems. In *Ecosystems and Human Well-being: Current State and Trends* 587–621. Millenium Ecosystem Assessment.

Grimley, D. A., Follmer, L. R., Hughes, R. E., & Solheid, P. A. (2003). Modern, Sangamon and Yarmouth soil development in loess of unglaciated southwestern Illinois. *Quaternary Science Reviews*, *22*(2), 225–244. https://doi.org/10.1016/S0277-3791(02)00039-2

Grimm, E. C., Watts, W. A., Jacobson, G. L., Hansen, B. C. S., Almquist, H. R., & Dieffenbacher-Krall, A. C. (2006). Evidence for warm wet Heinrich events in Florida. *Quaternary Science Reviews*, *25*, 2197–2211. https://doi.org/10.1016/j.quascirev.2006.04.008

Grüger, J. (1973). Studies on the late Quaternary vegetation history of northeastern Kansas. *Geological Society of America Bulletin*, *84*(1), 239–250.

Halfen, A. F., & Hasiotis, S. T. (2010a). Neoichnological study of the traces and burrowing behaviors of the western harvester ant Pogonomyrmex occidentalis (Insecta: Hymenoptera: Formicidae): paleopedogenic and paleoecological implications. *Palaios*, *25*(11), 703-720.

Halfen, A. F., & Hasiotis, S. T. (2010b). Downward thinking: rethinking the" up" in soil bioturbation. In *19th World Congress of Soil Science, Soil Solutions for a Changing World.* 1-6.

Hanson, P., Arbogast, A., Johnson, W., Joeckel, R., & Young, A. (2010). Megadroughts and late Holocene dune activation at the eastern margin of the Great Plains, north-central Kansas, USA. *Aeolian Research*, *1*(3), 101–110.

Hanson, P. R., Mason, J. A., Jacobs, P. M., & Young, A. R. (2015). Evidence for bioturbation of luminescence signals in eolian sand on upland ridgetops, southeastern Minnesota, USA. *Quaternary International*, *362*, 108–115. https://doi.org/10.1016/j.quaint.2014.06.039

Hasiotis, S. T., & Dubiel, R. F. (1994). Ichnofossil Tiering in Triassic Alluvial Paleosols: Implications for Pangean Continental Rocks and Paleoclimate, 311–317.

Hasiotis, S. T., & Platt, B. F. (2012). Exploring the sedimentary, pedogenic, and hydrologic factors that control the occurrence and role of bioturbation in soil formation and horizonation in continental deposits: an integrative approach. *The Sedimentary Record*, *10*(3), 4-9.

Heinrich, H. (1988). Origin and Consequences of Cyclic Ice Rafting in the Northeast Atlantic Ocean During the Past 130,000 Years. *Quaternary Research*, *29*(2), 142–152. https://doi.org/10.1016/0033-5894(88)90057-9

Heller, F., & Liu, T. (1986). Palaeoclimatic and sedimentary history from magnetic susceptibility of loess in China. *Geophysical Research Letters*, *13*(11), 1169–1172. https://doi.org/10.1029/GL013i011p01169

Henry, L. G., McManus, J. F., Curry, W. B., Roberts, N. L., Piotrowski, A. M., & Keigwin, L. D. (2016). North Atlantic ocean circulation and abrupt climate change during the last glaciation. *Science*, *353*(6298), 470–474. https://doi.org/10.1126/science.aaf5529

Higuera, P. E., Brubaker, L. B., Anderson, P. M., Hu, F. S., & Brown, T. A. (2009). Vegetation mediated the impacts of postglacial climate change on fire regimes in the south-central Brooks Range, Alaska. *Ecological Monographs*, *79*(2), 201–219. https://doi.org/10.1890/07-2019.1

Hofman, J. L., Carter, B. J., & Hill, M. (1992). Folsom occupation at the Waugh site in northwestern Oklahoma. *Current Research in the Pleistocene*, *9*, 22–25.

Holliday, V. T., Mayer, J. H., & Fredlund, G. G. (2008). Late Quaternary sedimentology and geochronology of small playas on the Southern High Plains, Texas and New Mexico, U.S.A. *Quaternary Research*, *70*, 11–25.

Hovan, S. A., Rea, D. K., Pisias, N. G., & Shackleton, N. J. (1989). A direct link between the China loess and marine δ18O records: aeolian flux to the north Pacific. *Nature*, *340*(6231), 296–298. https://doi.org/10.1038/340296a0

Hunt, C. P., Singer, M. J., Kletetschka, G., Tenpas, J., & Verosub, K. L. (1995). Effect of citrate-bicarbonate-dithionite treatment on fine-grained magnetite and maghemite. *Earth and Planetary Science Letters*, *130*(1), 87–94. https://doi.org/10.1016/0012-821X(94)00256-X

Hygnstrom, S. E., & Virchow, D. R. (1994). Prairie dogs. *The Handbook: Prevention and Control of Wildlife Damage*, 20.

Izett, G. A., & Wilcox, R. E. (1982). *Map showing localities and inferred distributions of the Huckleberry Ridge, Mesa Falls, and Lava Creek ash beds (Pearlette family ash beds) of Pliocene and Pleistocene age in the western United States and southern Canada* (USGS Numbered Series No. 1325). Retrieved from http://pubs.er.usgs.gov/publication/i1325

Jacobs, K. C., Fritz, S. C., & Swinehart, J. B. (2007). Lacustrine evidence for moisture changes in the Nebraska Sand Hills during Marine Isotope Stage 3. *Quaternary Research*, *67*(2), 246–254. https://doi.org/10.1016/j.yqres.2006.12.001

Jacobs, P. M., & Mason, J. A. (2007). Late Quaternary climate change, loess sedimentation, and soil profile development in the central Great Plains: A pedosedimentary model. *Geological Society of America Bulletin*, *119*(3–4), 462–475.

Jobbagy, E. G., & Jackson, R. B. (2000). The Vertical Distribution of Soil Organic Carbon and Its Relation to Climate and Vegetation. *Ecological Applications*, *10*(2), 423–436. https://doi.org/10.2307/2641104

Johnson, W. C., & Willey, K. L. (2000). Isotopic and Rock Magnetic Expression of Environmental Change at the Pleistocene-Holocene Transition in the Central Great Plains. *Quaternary International*, *67*, 89–106.

Johnson, W. C., Willey, K. L., Mason, J. A., & May, D. W. (2007a). Stratigraphy and environmental reconstruction at the middle Wisconsinan Gilman Canyon formation type locality, Buzzard's Roost, southwestern Nebraska, USA.

Quaternary Research, *67*(3), 474–486. https://doi.org/10.1016/j.yqres.2007.01.011

Johnson, W. C., Willey, K. L., & Macpherson, G. L. (2007b). Carbon isotope variation in modern soils of the tallgrass prairie: Analogues for the interpretation of isotopic records derived from paleosols. *Quaternary International*, *162*, 3–20. https://doi.org/10.1016/j.quaint.2006.10.036

Johnson, W. C., (1993). *Surficial geology and stratigraphy of Phillips County, Kansas, with emphasis on the Quaternary Period*. Kansas Geological Survey. Guidebook Series 5.

Karlstrom, E. T., Oviatt, C. G., & Ransom, M. D. (2008). Paleoenvironmental interpretation of multiple soil-loess sequences at Milford Reservoir, northeastern Kansas. *Catena*, *72*, 113–128.

King, J. E. (1973). Late Pleistocene Palynology and Biogeography of the Western Missouri Ozarks. *Ecological Monographs*, *43*(4), 539–565. https://doi.org/10.2307/1942305

Ku, T.-L., Bull, W. B., Freeman, S. T., & Knauss, K. G. (1979). Th230-U234 dating of pedogenic carbonates in gravelly desert soils of Vidal Valley, southeastern California. *GSA Bulletin*, *90*(11), 1063–1073. https://doi.org/10.1130/0016-7606(1979)90<1063:TDOPCI>2.0.CO;2

Kukla, G. J. (1977). Pleistocene land—sea correlations I. Europe. *Earth-Science Reviews*, *13*(4), 307–374. https://doi.org/10.1016/0012-8252(77)90125-8

Kurtén, B., & Anderson, E. (1980). *Pleistocene mammals of North America*. Columbia University Press.

Layzell, A. L., Mandel, R. D., Ludvigson, G. A., Rittenour, T. M., & Smith, J. J. (2015). Forces driving late Pleistocene (ca. 77–12 ka) landscape evolution in the Cimarron River valley, southwestern Kansas. *Quaternary Research*, *84*(1), 106–117. https://doi.org/10.1016/j.yqres.2015.05.003

Layzell, A. L., Mandel, R. D., Rittenour, T. M., Smith, J. J., Harlow, R. H., & Ludvigson, G. A. (2016). Stratigraphy, morphology, and geochemistry of late Quaternary buried soils on the High Plains of southwestern Kansas, USA. *CATENA*, *144*, 45–55. https://doi.org/10.1016/j.catena.2016.05.003

Le Borgne, E. (1955). Abnormal magnetic susceptibility of the top soil. *Ann. Geophys*, *11*, 399–419.

Leigh, D. S., & Knox, J. C. (1993). AMS Radiocarbon Age of the Upper Mississippi Valley Roxana Silt. *Quaternary Research*, *39*(3), 282–289. https://doi.org/10.1006/qres.1993.1035

Leigh, D. S., & Knox, J. C. (1994). Loess of the Upper Mississippi Valley Driftless Area. *Quaternary Research*, *42*(1), 30–40. https://doi.org/10.1006/qres.1994.1051

Leonard, A. B. (1951). Stratigraphic Zonation of the Peoria Loess in Kansas. *The Journal of Geology*, *59*(4), 323–332. https://doi.org/10.1086/625871

Leys, B., Brewer, S. C., McConaghy, S., Mueller, J., & McLauchlan, K. K. (2015). Fire history reconstruction in grassland ecosystems: amount of charcoal reflects local area burned. *Environmental Research Letters*, *10*(11), 114009. https://doi.org/10.1088/1748-9326/10/11/114009

Leys, B. A., Commerford, J. L., & McLauchlan, K. K. (2017). Reconstructing grassland fire history using sedimentary charcoal: Considering count, size and shape. *PLOS ONE*, *12*(4), e0176445. https://doi.org/10.1371/journal.pone.0176445

Löfverström, M., Caballero, R., Nilsson, J., & Kleman, J. (2014). Evolution of the large-scale atmospheric circulation in response to changing ice sheets over the last glacial cycle. *Climate of the Past*, *10*(4), 1453-1471.

Loope, D. B. (1986). Recognizing and Utilizing Vertebrate Tracks in Cross Section: Cenozoic Hoofprints from Nebraska. *PALAIOS*, *1*(2), 141–151. https://doi.org/10.2307/3514507

Ludlow, M. M., Troughton, J. H., & Jones, R. J. (1976). Technique for Determining Proportion of C3 and C4 Species in Plant Samples Using Stable Natural Isotopes of Carbon. *Journal of Agricultural Science*, *87*, 625–632.

Lynch-Stieglitz, J. (2017). The Atlantic Meridional Overturning Circulation and Abrupt Climate Change. *Annual Review of Marine Science*, *9*(1), 83–104. https://doi.org/10.1146/annurev-marine-010816-060415

Maat, P. B., & Johnson, W. C. (1996). Thermoluminescence and new 14C age estimates for late Quaternary loesses in southwestern Nebraska. *Geomorphology*, *17*, 115–128.

Machac, T. A., Zanner, C. W., & Geiss, C. E. (2007). Time dependent IRM acquisition as a tool to quantify the abundance of ultrafine superparamagnetic magnetite in loessic soils. *Geophysical Journal International*, *169*(2), 483–489. https://doi.org/10.1111/j.1365-246X.2007.03355.x

Maher, B. A. (1998). Magnetic properties of modern soils and Quaternary loessic paleosols: paleoclimatic implications. *Palaeogeography, Palaeoclimatology, Palaeoecology*, *137*(1), 25–54. https://doi.org/10.1016/S0031-0182(97)00103-X

Maher, B. A. (2011). The magnetic properties of Quaternary aeolian dusts and sediments, and their palaeoclimatic significance. *Aeolian Research*, *3*(2), 87–144. https://doi.org/10.1016/j.aeolia.2011.01.005

Maher, B. A. (2016). Palaeoclimatic records of the loess/palaeosol sequences of the Chinese Loess Plateau. *Quaternary Science Reviews*, *154*, 23–84. https://doi.org/10.1016/j.quascirev.2016.08.004

Maher, B. A., & Thompson, R. (1991). Mineral magnetic record of the Chinese loess and paleosols. *Geology*, *19*(1), 3–6. https://doi.org/10.1130/0091-7613(1991)019<0003:MMROTC>2.3.CO;2

Mandel, R., Bettis, E. A., & Hanson, P. R. (2016). Characteristics and Geochronology of the Severance Formation: a new mid- through late Wisconsinan Lithostratigraphic Unit in the Eastern Plains of North America. Geological Society of America Abstracts with Programs 48(7). https://doi.org/10.1130/abs/2016AM-286301

Marin-Spiotta, E., Chaopricha, N. T., Plante, A. F., Diefendorf, A. F., Mueller, C. W., Grandy, A. S., & Mason, J. A. (2014). Long-term stabilization of deep soil carbon by fire and burial during early Holocene climate change. *Nature Geoscience; London*, *7*(6), 428–432. http://dx.doi.org/10.1038/ngeo2169

Markewich, H. W., Wysocki, D. A., Pavich, M. J., & Rutledge, E. M. (2011). Age, genesis, and paleoclimatic interpretation of the Sangamon/Loveland complex in the Lower Mississippi Valley, U.S.A. *GSA Bulletin*, *123*(1–2), 21–39. https://doi.org/10.1130/B30208.1

Mason, J. A. (1998). Relative rates of Peoria Loess accumulation and pedogenic processes: Implications for paleoclimatic inference. *Quaternary International*, *51–52*, 169–174. https://doi.org/10.1016/S1040-6182(97)00042-6

Mason, J. A. (2001). Transport Direction of Peoria Loess in Nebraska and Implications for Loess Sources on the Central Great Plains. *Quaternary Research*, *56*(1), 79–86. https://doi.org/10.1006/qres.2001.2250

Mason, J. A., Nater, E. A., & Hobbs, H. C. (1994). Transport Direction of Wisconsinan Loess in Southeastern Minnesota. *Quaternary Research*, *41*(1), 44–51. https://doi.org/10.1006/qres.1994.1005

Mason, J. A., Jacobs, P. M., Hanson, P. R., Miao, X., & Goble, R. J. (2003a). Sources and paleoclimatic significance of Holocene Bignell Loess, central Great Plains, USA. *Quaternary Research*, *60*, 330–339.

Mason, J. A., Jacobs, P. M., Greene, R. S. B., & Nettleton, W. D. (2003b). Sedimentary aggregates in the Peoria Loess of Nebraska, USA. *Catena*, *53*, 377–397. https://doi.org/10.1016/S0341-8162(03)00073-0

Mason, J. A., Joeckel, R. M., & Bettis, E. A. (2007). Middle to Late Pleistocene loess record in eastern Nebraska, USA, and implications for the unique nature of Oxygen Isotope Stage 2. *Quaternary Science Reviews*, *26*, 773–792. https://doi.org/10.1016/j.quascirev.2006.10.007

Mason, J. A., Miao, X. D., Hanson, P. R., Johnson, W. C., Jacobs, P. M., & Goble, R. J. (2008). Loess record of the Pleistocene-Holocene transition on the northern and central Great Plains, USA. *Quaternary Science Reviews*, *27*, 1772–1783. https://doi.org/10.1016/j.quascirev.2008.07.004

McLean, J. A. (2010). *A Reassessment of the Significance of the Coffey Site (14PO1), Tuttle Creek Lake, Pottawatomie County, Kansas* (Thesis). University of Kansas. Retrieved from https://kuscholarworks.ku.edu/handle/1808/6973

Muhs, D. R., Aleinikoff, J. N., Stafford, T. W., Kihl, R., Been, J., Mahan, S. A., & Cowherd, S. (1999). Late Quaternary loess in northeastern Colorado: Part I - Age and paleoclimatic significance. *Geological Society of America Bulletin*, *111*, 1861–1875.

Muhs, D. R., & Bettis, E. A. (2003). Quaternary loess-paleosol sequences as examples of climate-driven sedimentary extremes. In *Geological Society of America Special Paper 370*, 53–73. Boulder, CO, USA: Geological Society of America.

Muhs, D. R., Bettis, E. A., Aleinikoff, J. N., McGeehin, J. P., Beann, J., Skipp, G., Marshall, B. D., Roberts, H. M., Johnson, W. C., Benton, R. (2008). Origin and paleoclimatic significance of late Quaternary loess in Nebraska: Evidence from stratigraphy, chronology, sedimentology, and geochemistry. *Geological Society of America Bulletin*, *120*, 1378–1407. https://doi.org/10.1130/B26221.1

Mullins, C. E. (1977). Magnetic Susceptibility of the Soil and Its Significance in Soil Science – a Review. *Journal of Soil Science*, *28*(2), 223–246. https://doi.org/10.1111/j.1365-2389.1977.tb02232.x

Munyikwa, K., Feathers, J. K., Rittenour, T. M., & Shrimpton, H. K. (2011). Constraining the Late Wisconsinan retreat of the Laurentide ice sheet from western Canada using luminescence ages from postglacial aeolian dunes. *Quaternary Geochronology*, *6*(3), 407–422. https://doi.org/10.1016/j.quageo.2011.03.010

Murray, A., & Wintle, A. (2000). Luminescence dating of quartz using an improved single-aliquot regenerative-dose protocol. *Radiation Measurements*, *32*, 57–73.

Nordt, L. C., Boutton, T. W., Hallmark, C. T., & Waters, M. R. (1994). Late Quaternary vegetation and climate changes in Central Texas based on the isotopic composition of organic carbon. *Quaternary Research*, *41*, 109–120.

Ode, D. J., Tieszen, L. L., & Lerman, J. C. (1980). The Seasonal Contribution of C3 and C4 Plant-Species to Primary Production in a Mixed Prairie. *Ecology*, *61*, 1304–1311.

O'Leary, M. H. (1981). Carbon isotope fractionation in plants. *Phytochemistry*, *20*(4), 553–567. https://doi.org/10.1016/0031-9422(81)85134-5

O'Leary, M. H. (1988). Carbon Isotopes in Photosynthesis. *BioScience*, *38*(5), 328–336. https://doi.org/10.2307/1310735

Olson, C. G., & Nettleton, W. D. (1998). Paleosols and the effects of alteration. *Quaternary International*, *51–52*, 185–194.

Orgeira, M. J., Egli, R., & Compagnucci, R. H. (2011). A quantitative model of magnetic enhancement in loessic soils. In *The Earth's Magnetic Interior,* 361–397. Springer.

Osmond, C. B., Winter, K., & Ziegler, H. (1982). Functional Significance of Different Pathways of CO2 Fixation in Photosynthesis. In *Physiological Plant Ecology II,* 479–547. Springer, Berlin, Heidelberg. https://doi.org/10.1007/978-3-642-68150-9_16

Paces, J. B., Neymark, L. A., Marshall, B. D., Whelan, J. F., & Peterman, Z. E. (2001). Ages and Origins of Calcite and Opal in Exploratory Studies Facility Tunnel, Yucca Mountain, Nevada. *Water Resources Investigations Report. United States Geological Survey*, (4049), 108.

Peterson, L. C., & Haug, G. H. (2006). Variability in the mean latitude of the Atlantic Intertropical Convergence Zone as recorded by riverine input of sediments to the Cariaco Basin (Venezuela). *Palaeogeography, Palaeoclimatology, Palaeoecology*, *234*(1), 97–113. https://doi.org/10.1016/j.palaeo.2005.10.021

Piperno, D. R. (2006). *Phytoliths: A Comprehensive Guide for Archaeologists and Paleoecologists*. Rowman Altamira.

Pye, K., Winspear, N. R., & Zhou, L. P. (1995). Thermoluminescence ages of loess and associated sediments in central Nebraska, USA. *Palaeogeography, Palaeoclimatology, Palaeoecology*, *118*, 73–87.

Rea, D. (1994). The Paleoclimatic Record Provided by Eolian Deposition in the Deep Sea: The Geologic History of Wind. *Reviews of Geophysics*, *32*(2), 159–195. https://doi.org/10.1029/93RG03257

Reed, E. C., & Dreeszen, V. H. (1965). *Revision of the classification of the Pleistocene deposits of Nebraska*. Lincoln: University of Nebraska, Conservation and Survey Division.

Rittenour, T. M., Goble, R. J., & Blum, M. D. (2005). Development of an OSL chronology for Late Pleistocene channel belts in the lower Mississippi valley, USA. *Quaternary Science Reviews*, *24*, 2539–2554.

Roberts, H. M., Muhs, D. R., Wintle, A. G., Duller, G. A. T., & Bettis, E. A. (2003). Unprecedented last-glacial mass accumulation rates determined by luminescence dating of loess from western Nebraska. *Quaternary Research*, *59*(3), 411–419. https://doi.org/10.1016/S0033-5894(03)00040-1

Rousseau, D.-D., & Kukla, G. (1994). Late Pleistocene climate record in the Eustis loess section, Nebraska, based on land snail assemblages and magnetic susceptibility. *Quaternary Research*, *42*(2), 176–187.

Ruhe, R. V. (1983). Depositional environment of late Wisconsin loess in the midcontinental United States. *Late-Quaternary Environments of the United States*, *1*, 130–137.

Ruhe, R.V., Miller, G. A., & Vreeken, W. J. (1971). Paleosols, Loess Sedimentation, and Soil Stratigraphy. In D. H. Yaalon (Ed.), *Paleopedology: Origin, Nature, and Dating of Paleosols,* 41–62. Jerusalem: Israel Universities Press.

Ruth, U., Wagenbach, D., Steffensen, J. P., & Bigler, M. (2003). Continuous record of microparticle concentration and size distribution in the central Greenland NGRIP ice core during the last glacial period. *Journal of Geophysical Research: Atmospheres*, *108*(3). https://doi.org/10.1029/2002JD002376

Salomé, C., Nunan, N., Pouteau, V., Lerch, T. Z., & Chenu, C. (2009). Carbon dynamics in topsoil and in subsoil may be controlled by different regulatory mechanisms. *Global Change Biology*, *16*(1), 416–426. https://doi.org/10.1111/j.1365-2486.2009.01884.x

Sandström, H., Reeder, S., Bartha, A., Birke, M., Berge, F., Davidsen, B., Grimstvedt, A., Hagel-Brunnström, M. L., Kantor, W., Kallio, E. (2005). Sample preparation and analysis. *FOREGS Geochemical Atlas of Europe, Part 1*.

Schultz, C. B., & Stout, T. M. (1945). Pleistocene loess deposits of Nebraska. *American Journal of Science*, *243*, 231–244.

Schultz, C. B. (1934). The Pleistocene mammals of Nebraska. *Bulletin of the University of Nebraska State Museum*, *1*(41), 19–37.

Serefiddin, F., Schwarcz, H. P., Ford, D. C., & Baldwin, S. (2004). Late Pleistocene paleoclimate in the Black Hills of South Dakota from isotope records in speleothems. *Palaeogeography, Palaeoclimatology, Palaeoecology*, *203*, 1–17.

Shackleton, N. J., & Opdyke, N. D. (1973). Oxygen Isotope and Palaeomagnetic Stratigraphy of Equatorial Pacific Core V28-238: Oxygen Isotope Temperatures and Ice Volumes on a 10^5 Year and 10^6 Year Scale. *Quaternary Research*, *3*(1), 39–55. https://doi.org/10.1016/0033-5894(73)90052-5

Sheldon, N. D., & Tabor, N. J. (2009). Quantitative paleoenvironmental and paleoclimatic reconstruction using paleosols. *Earth-Science Reviews*, *95*(1), 1–52. https://doi.org/10.1016/j.earscirev.2009.03.004

Sherman, S. A., & Johnson, W. C. (2006). Evaluation and geoarchaeological analysis of the Mandell (14RY6175) and Hall (14RY6176) sites and shovel testing of

site 14RY5175 at Fort Riley, Kansas. *Center for Environment of Military Lands TPS*, 06–13.

Singer, M. J., & Verosub, K. L. (2007). Magnetic Mineral Analysis. *In: Elias S (ed) The encyclopedia of Quaternary sciences* (pp. 2096–2102).

Singer, M. J., & Fine, P. (1989). Pedogenic Factors Affecting Magnetic Susceptibility of Northern California Soils. *Soil Science Society of America Journal*, *53*(4), 1119–1127. https://doi.org/10.2136/sssaj1989.03615995005300040023x

Smith, G. D. (1942). *Illinois loess: variations in its properties and distribution, a pedologic interpretation*. Urbana, Ill.: University of Illinois, Agricultural Experiment Station. Retrieved from http://hdl.handle.net/2142/3113

Smith, J. J., Hasiotis, S. T., Kraus, M. J., & Woody, D. T. (2008). Naktodemasis bowni: New ichnogenus and ichnospecies for adhesive meniscate burrows (AMB), and paleoenvironmental implications, Paleogene Willwood Formation, Bighorn Basin, Wyoming. *Journal of Paleontology*, *82*(2), 267–278. https://doi.org/10.1666/06-023.1

Stevenson, F. J., & Cole, M. A. (1999). *Cycles of Soils: Carbon, Nitrogen, Phosphorus, Sulfur, Micronutrients*. John Wiley & Sons.

Stuiver, M., & Grootes, P. M. (2000). GISP2 Oxygen Isotope Ratios. *Quaternary Research*, *53*(3), 277–284. https://doi.org/10.1006/qres.2000.2127

Svensson, A., Andersen, K. K., Bigler, M., Clausen, H. B., Dahl-Jensen, D., Davies, S. M., Johnsen, S. J., Muscheler, R., Rasmussen, S.O., Röthlisberger, R., Peder-Steffenson, J., Vinther, B. M. (2006). The Greenland Ice Core Chronology 2005,

15–42ka. Part 2: comparison to other records. *Quaternary Science Reviews*, *25*(23), 3258–3267. https://doi.org/10.1016/j.quascirev.2006.08.003

Swineford, A., & Frye, J. C. (1951). Petrography of the Peoria Loess in Kansas. *The Journal of Geology*, *59*(4), 306–322. https://doi.org/10.1086/625870

Taylor, R. M., Maher, B. A., & Self, P. G. (1987). Magnetite in soils: I. The synthesis of single-domain and superparamagnetic magnetite. *Clay Minerals*, *22*(4), 411–422.

Teeri, J. A., & Stowe, L. G. (1976). Climatic Patterns and Distribution of C4 Grasses in North-America. *Oecologia*, *23*, 1–12.

Thorp, J., Johnson, W. M., & Reed, E. C. (1951). Some Post-Pliocene Buried Soils of Central United-States. *Journal of Soil Science*, *2*, 1–19.

Tobin, R. J. (2004a). Ichnology of a late Pleistocene ichnofabric, Nebraska, USA. *Palaeogeography, Palaeoclimatology, Palaeoecology*, *215*(1), 111–123. https://doi.org/10.1016/j.palaeo.2004.08.007

Tobin, R. J. (2004b). Taphonomy of ground squirrel remains in a Late Pleistocene ichnofabric, Nebraska, USA. *Palaeogeography, Palaeoclimatology, Palaeoecology*, *214*(1), 125–134. https://doi.org/10.1016/j.palaeo.2004.07.025

Torrent, J., Barrón, V., & Liu, Q. (2006). Magnetic enhancement is linked to and precedes hematite formation in aerobic soil. *Geophysical Research Letters*, *33*(2). https://doi.org/10.1029/2005GL024818

Újvári, G., Stevens, T., Molnár, M., Demény, A., Lambert, F., Varga, G., Jull, A. J., Páll-Gergely, B., Buylaert, J-P., Kovács, J. (2017). Coupled European and Greenland

last glacial dust activity driven by North Atlantic climate. *Proceedings of the National Academy of Sciences*, *114*(50), 10632–10638. https://doi.org/10.1073/pnas.1712651114

van der Werf, G. R., Randerson, J. T., Giglio, L., Gobron, N., & Dolman, A. J. (2008). Climate controls on the variability of fires in the tropics and subtropics. *Global Biogeochemical Cycles*, *22*(3). https://doi.org/10.1029/2007GB003122

Van Meerbeeck, C., Renssen, H., & Roche, D. (2009). How did marine isotope stage 3 and Last Glacial Maximum climates differ? Perspectives from equilibrium simulations. *Climates of the Past, 5,* 33-51

Virchow, D. R., & Hygnstrom, S. E. (2002). Distribution and Abundance of Black-tailed Prairie Dogs in the Great Plains: a Historical Perspective. *Great Plains Research*, *12*(2), 197–218.

Voelker, A. H. L., & workshop participants. (2002). Global distribution of centennial-scale records for Marine Isotope Stage (MIS) 3: a database. *Quaternary Science Reviews*, *21*, 1185–1212.

Wang, Z., & Mysak, L. A. (2006). Glacial abrupt climate changes and Dansgaard-Oeschger oscillations in a coupled climate model. *Paleoceanography*, *21*(2). https://doi.org/10.1029/2005PA001238

Wells, P. V., & Stewart, J. D. (1987). Cordilleran-boreal Taiga and Fauna on the Central Great Plains of North America, 14,000-18,000 Years Ago. *The American Midland Naturalist*, *118*(1), 94–106. https://doi.org/10.2307/2425632

Werner, C. M., Mason, J. A., & Hanson, P. R. (2011). Non-linear connections between dune activity and climate in the High Plains, Kansas and Oklahoma, USA. *Quaternary Research*, *75*(1), 267–277. https://doi.org/10.1016/j.yqres.2010.08.001

Wilding, L. P., & Drees, L. R. (1971). Biogenic Opal in Ohio Soils 1. *Soil Science Society of America Journal*, *35*(6), 1004–1010. https://doi.org/10.2136/sssaj1971.03615995003500060041x

Wills, S. A., Burras, C. L., & Sandor, J. A. (2007). Prediction of Soil Organic Carbon Content Using Field and Laboratory Measurements of Soil Color. *Soil Science Society of America Journal*, *71*(2), 380–388. https://doi.org/10.2136/sssaj2005.0384

Woodburn, T. L., Johnson, W. C., Mason, J. A., Bozarth, S. R., & Halfen, A. F. (2017). Vegetation dynamics during the Pleistocene–Holocene transition in the central Great Plains, USA. *The Holocene*, *27*(1), 155–163. https://doi.org/10.1177/0959683616652710

Wunsch, C. (2006). Abrupt climate change: An alternative view. *Quaternary Research*, *65*(2), 191–203. https://doi.org/10.1016/j.yqres.2005.10.006

Yang, Y., Mason, J. A., Zhang, H., Lu, H., Ji, J., Chen, J., & Liu, L. (2017). Provenance of loess in the central Great Plains, U.S.A. based on Nd-Sr isotopic composition, and paleoenvironmental implications. *Quaternary Science Reviews*, *173*, 114–123. https://doi.org/10.1016/j.quascirev.2017.08.009

Tables

Table 1. Numerical AMS ages from the GCF at the RCL.

Stratigraphic Unit	Sample ID[a]	Depth (cm)	^{14}C age ± 2σ (ka)
GCF S2			
Profile	RLP14	20	**37,610 ± 1,705**
	RLP11	130	**44,522 ± 3,129**
	RLCS12	340	**36,714 ± 1,589**
	RLCS13	371	**40,125 ± 1,919**
	RLCS14	407	**38,323 ± 2,010**
	RLCS15	446	**35,324 ± 1,096**
Core	RLE14	634	**32,974 ± 1,035**
	RLE15	665	**31,560 ± 763**
	RLE16	690	**34,167 ± 857**
	RLE17	712	**45,662 ± 4,076**
	RCPS11	35	**33,956 ± 270**
	RCPS13	100	**33,963 ± 271**
	RCPS16	195	**39,137 ± 552**
GCF S1			
Core	RLCS1B	225	**30,156 ± 481**
	RLE13	431	**24,932 ± 446**

[a] see Figure 4 for sample locations.

Table 2. Numerical OSL age information from the RCL.

Stratigraphic Unit	Sample ID[a]	Depth (m)	Number of aliquots[b]	Dose rate (Gy/ka)	D_E[c] ± 2σ (Gy)	OD[d] (%)	OSL age ± 2σ (ka)
Basal Sand	RCPW 2-7	6.8	19 (24)	2.89 ± 0.27	156.11 ± 15.03	17.6 ± 4	**54.06 ± 8.71**
	RCPS 1-9	4	19 (30)	2.24 ± 0.17	114.83 ± 16.65	27.5 ± 5.8	**51.16 ± 9.57**
Loveland Loess	RCPS 1-8	3.15	23 (30)	2.28 ± 0.32	137.96 ± 10.59	14.7 ± 3.3	**60.50 ± 10.88**
Sangamon Soil	RCPW 1-4	2.7	24 (33)	3.01 ± 0.20	184.74 ± 13.79	14.5 ± 3.2	**61.34 ± 8.05**
	RCPW 1-3	1.9	18 (19)	3.24 ± 0.22	155.86 ± 17.33	20.7 ± 4.4	**48.05 ± 7.44**
	RCPS 1-7	2.5	17 (29)	3.38 ± 0.23	147.46 ± 13.46	13.3 ± 4.3	**43.59 ± 6.17**
Detrital Unit	RCPW 2-3	4.24	17 (22)	2.57 ± 0.22[e]	82.10 ± 10.38	22.1 ± 5.1	**31.99 ± 5.60**
Peoria Loess	RCPW 2-4	3.43	20 (20)	3.20 ± 0.30	87.67 ± 6.31	12.2 ± 3.3	**27.43 ± 3.96**
	RCPW 2-5	2.12	19 (20)	3.11 ± 0.27	80.99 ± 6.49	14.5 ± 3.4	**26.01 ± 3.76**
	RCPW 2-6	1.5	19 (20)	3.28 ± 0.26	54.52 ± 3.55	10.9 ± 3.0	**16.60 ± 2.21**

[a] see Figure 4 for sample locations.
[b] Age produced using single-aliquot regenerative-dose from Murray and Wintle (2000) on 1-2 mm aliquots of quatz sand. Number of aliquots used in age calculation and number of aliquots analyzed in parentheses.
[c] Equivalent dose (DE) calculated using the Central Age Model (CAM) of Galbraith and Roberts (2012).
[d] Overdispersion (OD) represents variance in DE data beyond measurement uncertainties, OD >20% may indicate significant scatter due to depositional or post-depositional processes.
[e] Dose rate average of three samples

Figures

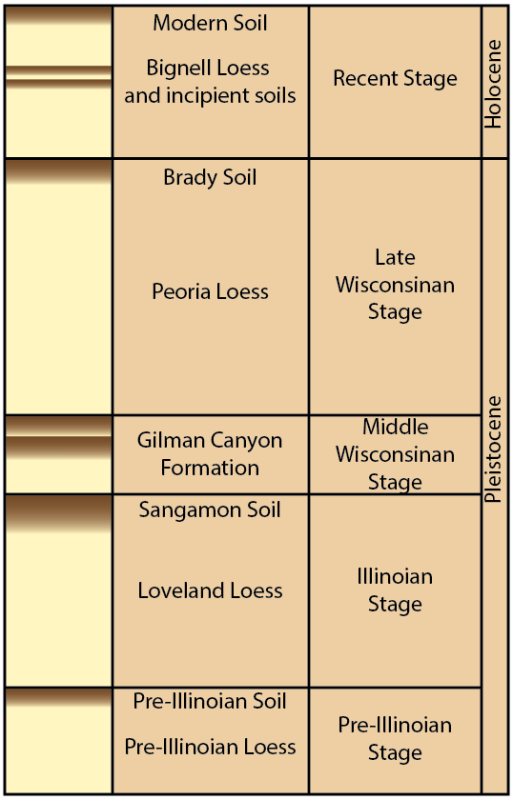

Figure 1. Central Great Plains Late Quaternary loess sequence. Figure represents a typical loess sequence but thickness and presence of units varies throughout the Central Great Plains. Modified from Johnson et al. (2007a) and Woodburn et al. (2017).

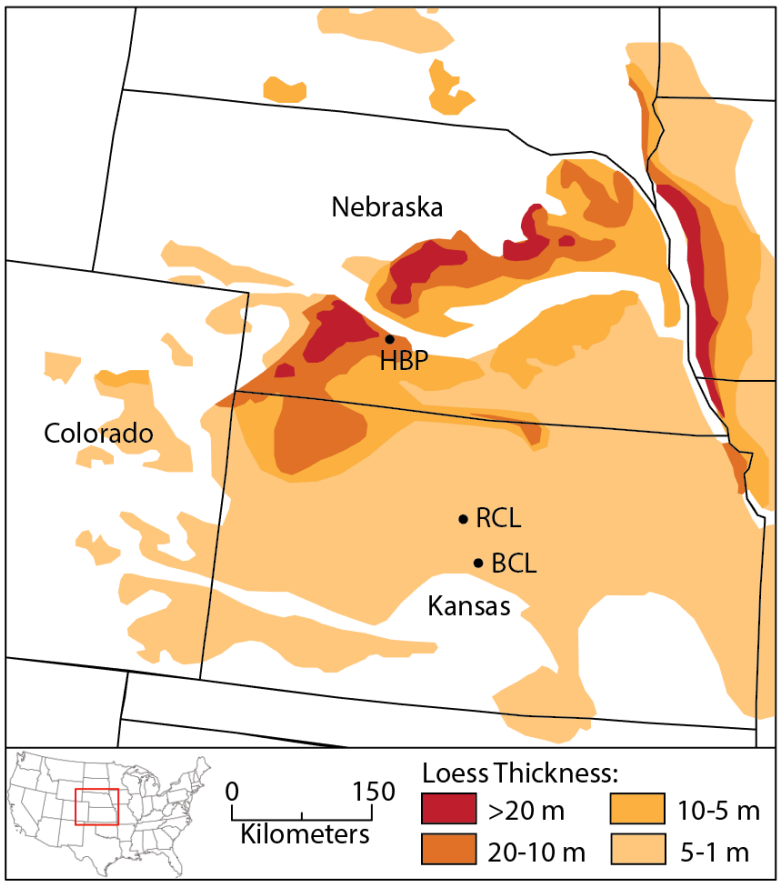

Figure 2. Extent and thickness of Peoria Loess, from the last glacial period in the Central Great Plains. Russell County Landfill (RCL), the focus of this study along with Hueftle Borrow Pit (HBP) and Barton County Landfill (BCL) are shown. After Bettis et al. (2003).

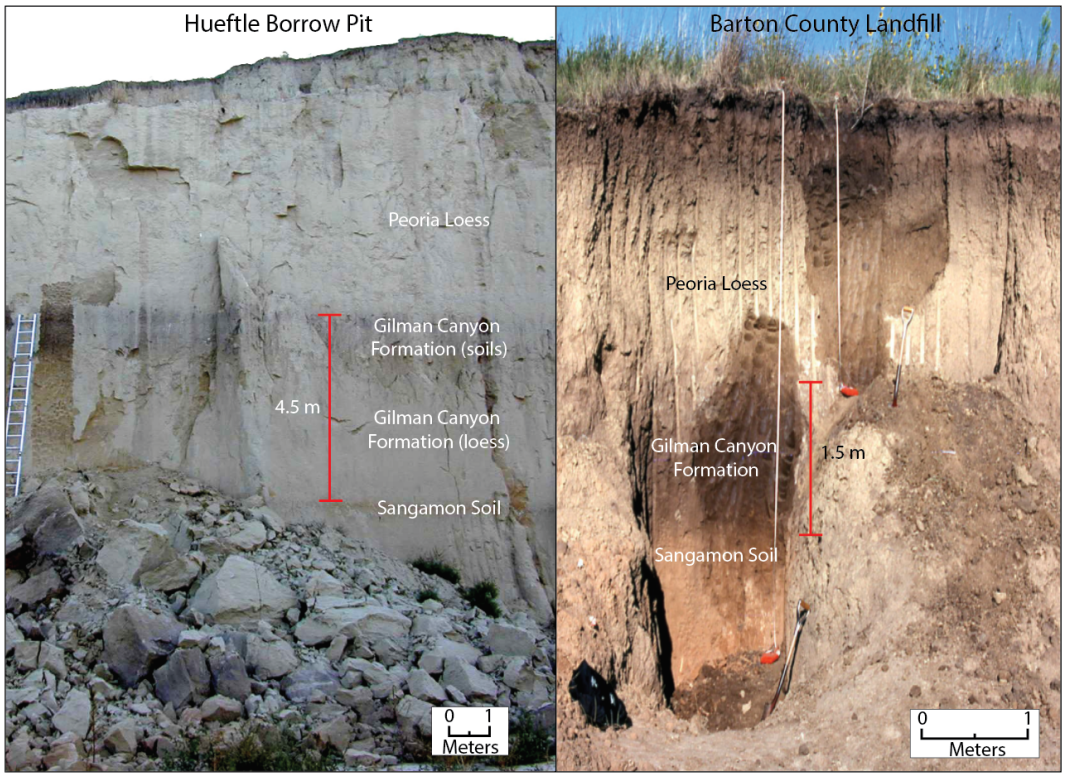

Figure 3. Loess unit thickness comparison between a site in the proximal loess plume in southwestern Nebraska, Hueftle Borrow Pit, and the distal loess plume in central Kansas at the Barton County Landfill. Peoria Loess (truncated and overlain by spoil at Hueftle), Gilman Canyon Formation, and Sangamon Soil are labeled to highlight the extent to which these units change over geographical space. Gilman Canyon Formation, appears as two loess units and two soils at Hueftle Borrow Pit, located on the south bluff of the Platte River in Nebraska, where the unit is at least 4.5 m thick, and as a single 1.5 m thick soil, with no apparent unaltered Gilman Canyon Formation loess, at the Barton County Landfill ~80 km south of Russell County landfill.

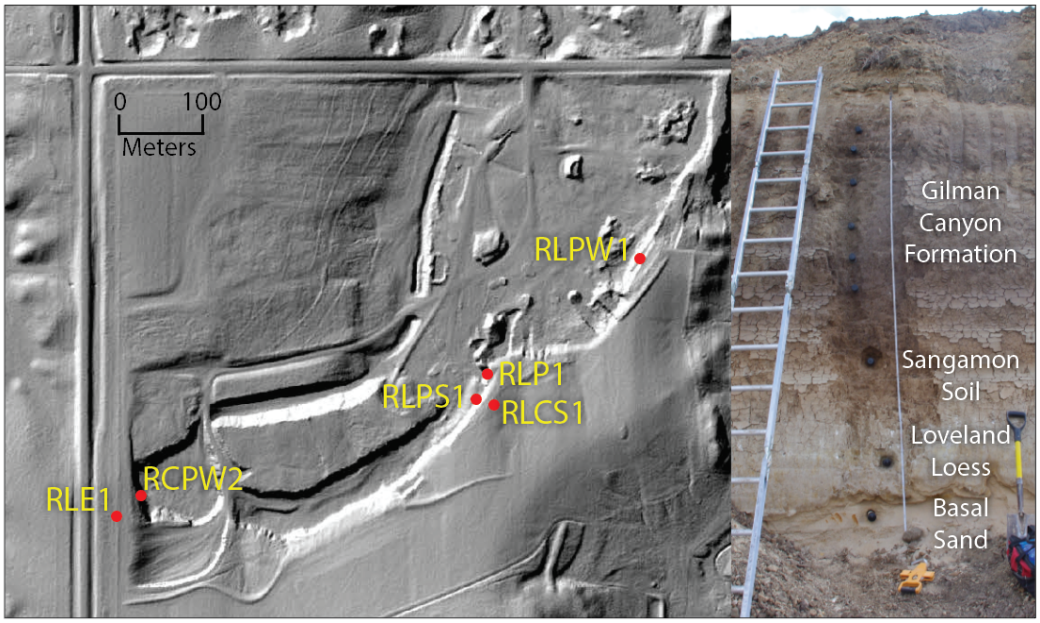

Figure 4. Shaded relief map of Russell County Landfill created with 2012 LiDAR data. Core and profile locations indicated by red points with respective labels. RLPS1 served as reference exposure and shown on right (the overlying Peoria Loess, GCF S1, and detrital unit are truncated at this exposure).

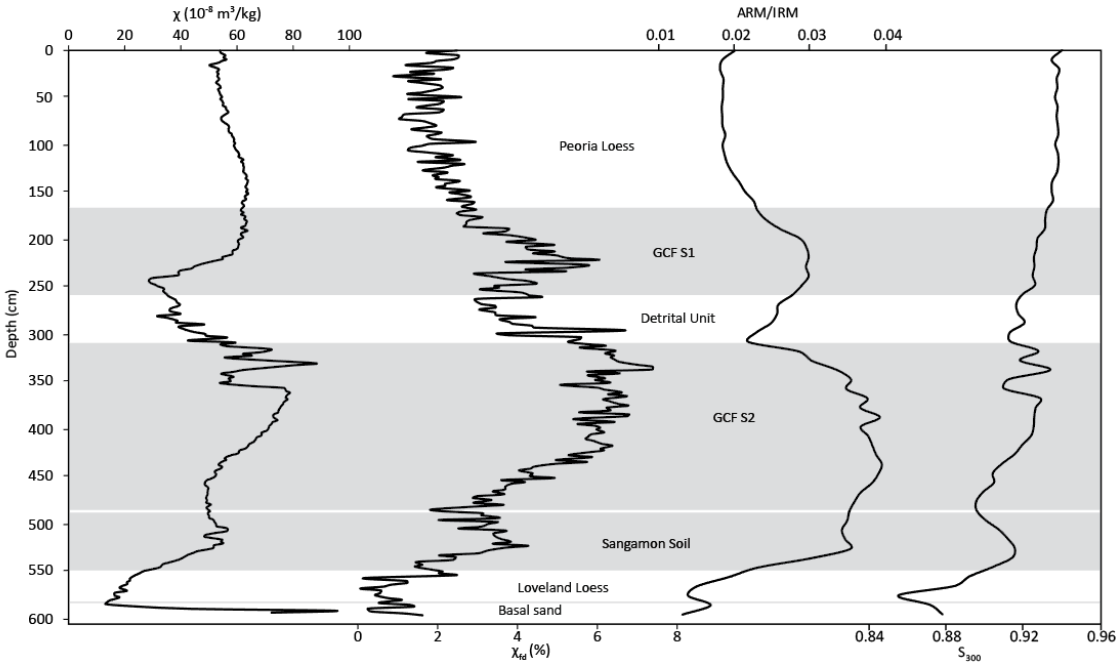

Figure 5. Enviromagnetic data including χ, χ_{fd}, ARM/IRM, and S_{300} derived from core samples. Gray shaded zones indicate the location of soils in the profile.

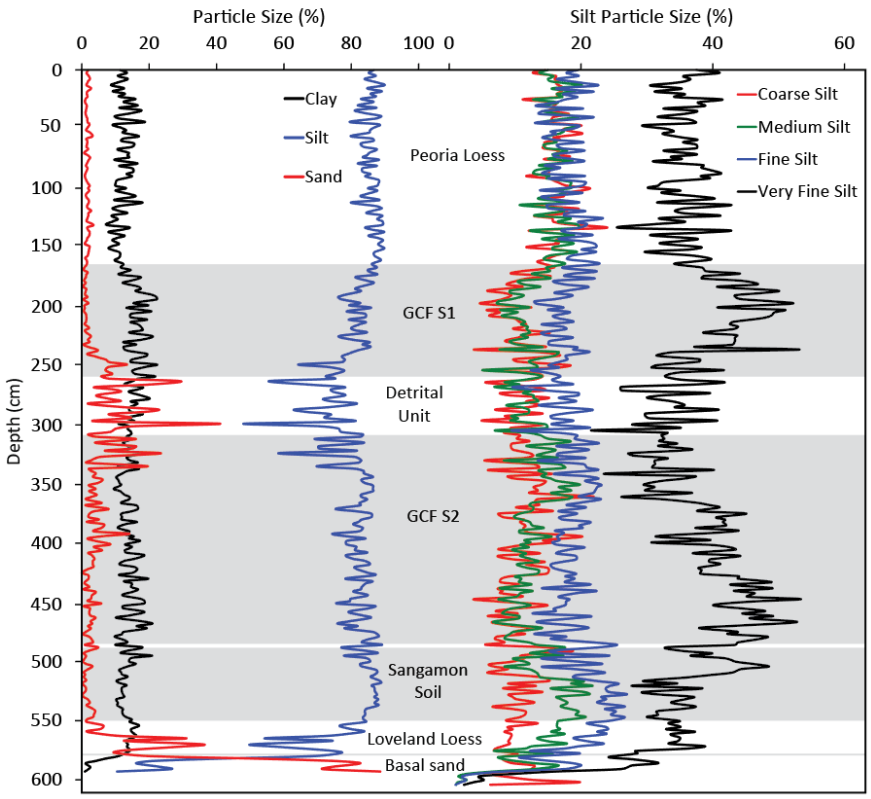

Figure 6. Particle size parameters obtained from core plotted with labeled stratigraphy. Percent of sand, silt, and clay displayed on left, and silt fraction further divided into percent very fine silt, fine silt, medium silt, and coarse silt on right. Gray-shaded zones indicate soils.

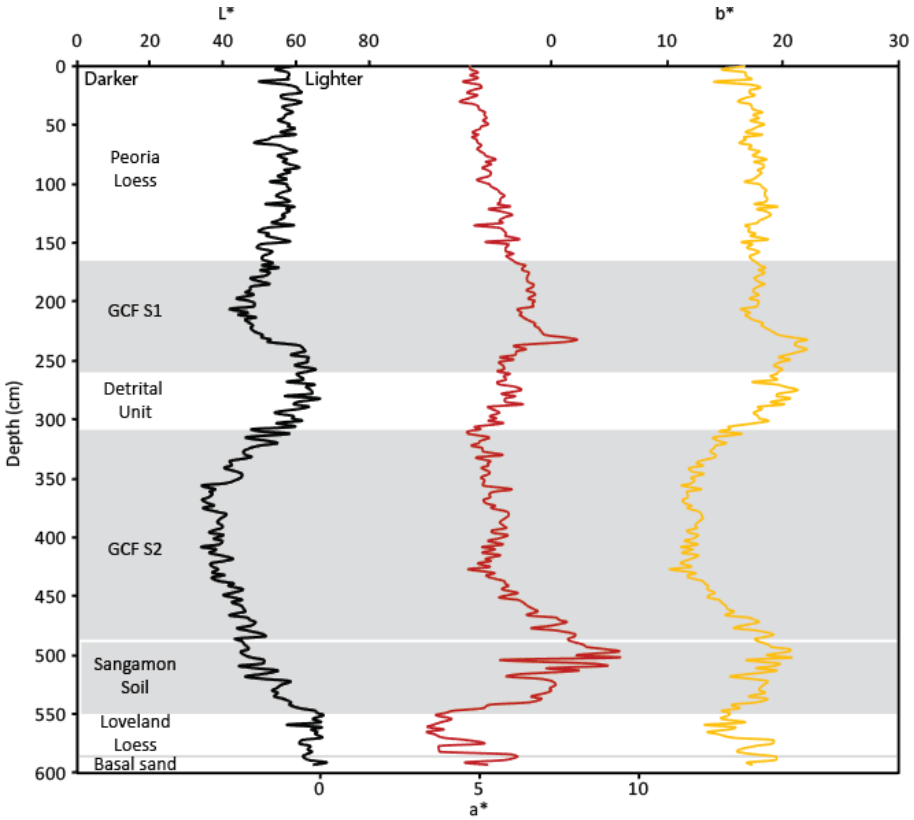

Figure 7. Core-derived spectral color using the CIELAB color system (*L**, *a**, and *b**) plotted with depth and stratigraphic units. Gray-shaded zones indicate soils.

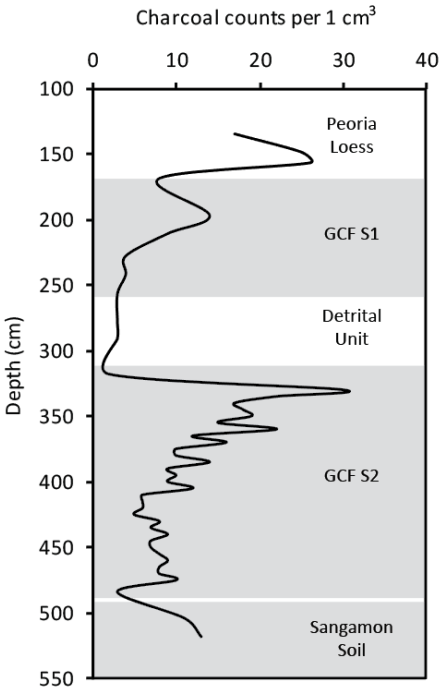

Figure 8. Sedimentary charcoal fragment counts for charcoal pieces > 63 µm plotted with depth and labeled stratigraphy. Gray-shaded zones indicate soils.

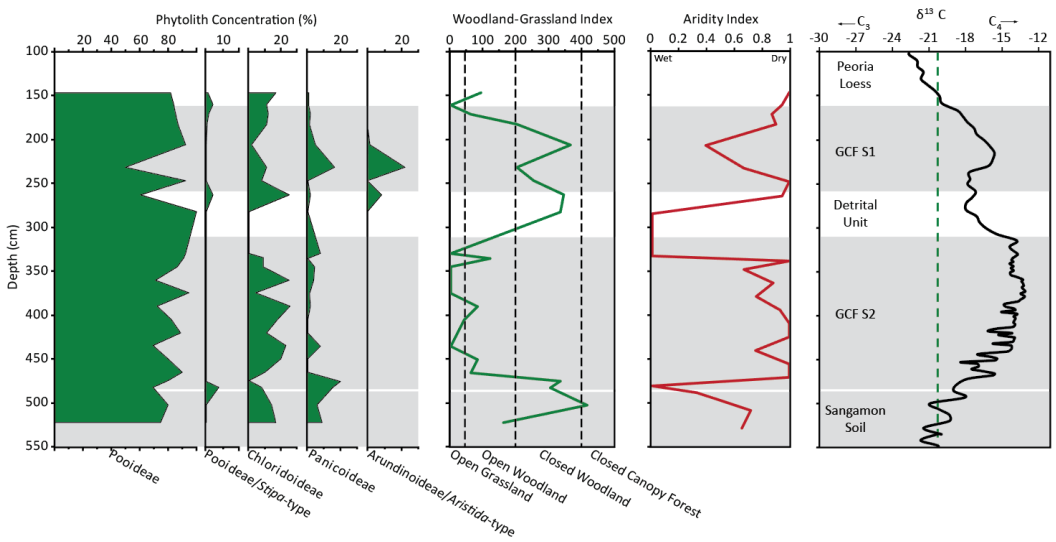

Figure 9. Phytolith concentrations, woodland-grassland index, aridity index, and $\delta^{13}C$ obtained from core samples with stratigraphy. Gray-shaded zones indicate soils. Woodland-grassland index modeled after Cordova et al. (2011), and aridity index modeled after Diester-Haass et al. (1973).

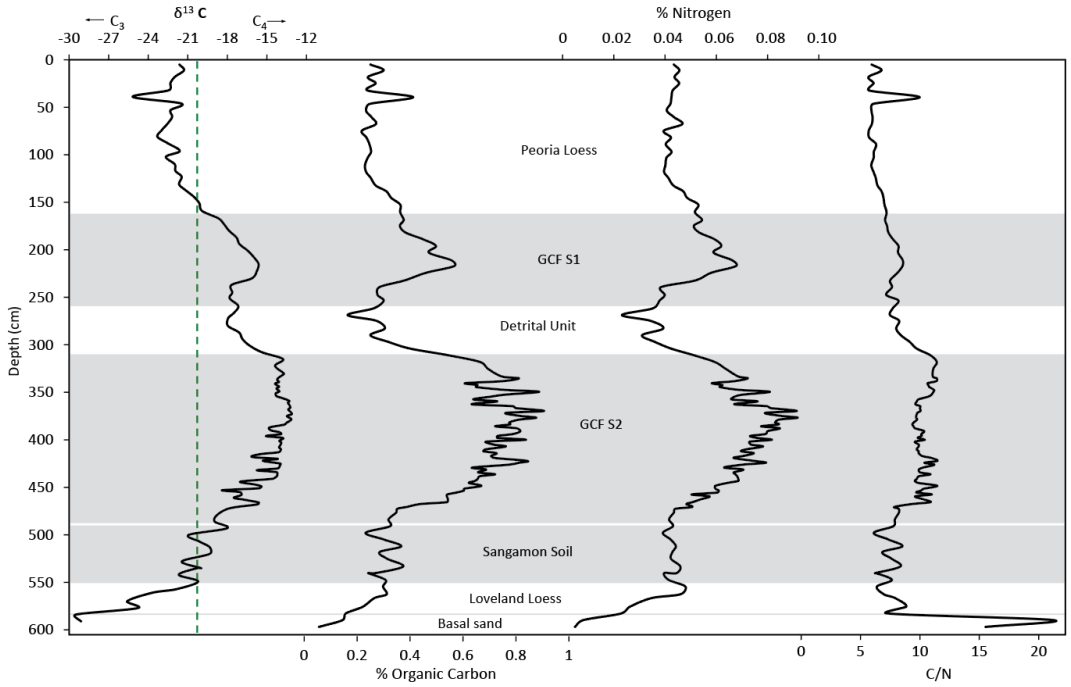

Figure 10. Stable carbon isotope ($\delta^{13}C$), percent organic carbon, percent nitrogen, and C/N ratio derived from core samples with stratigraphy. Gray-shaded zones indicate soils.

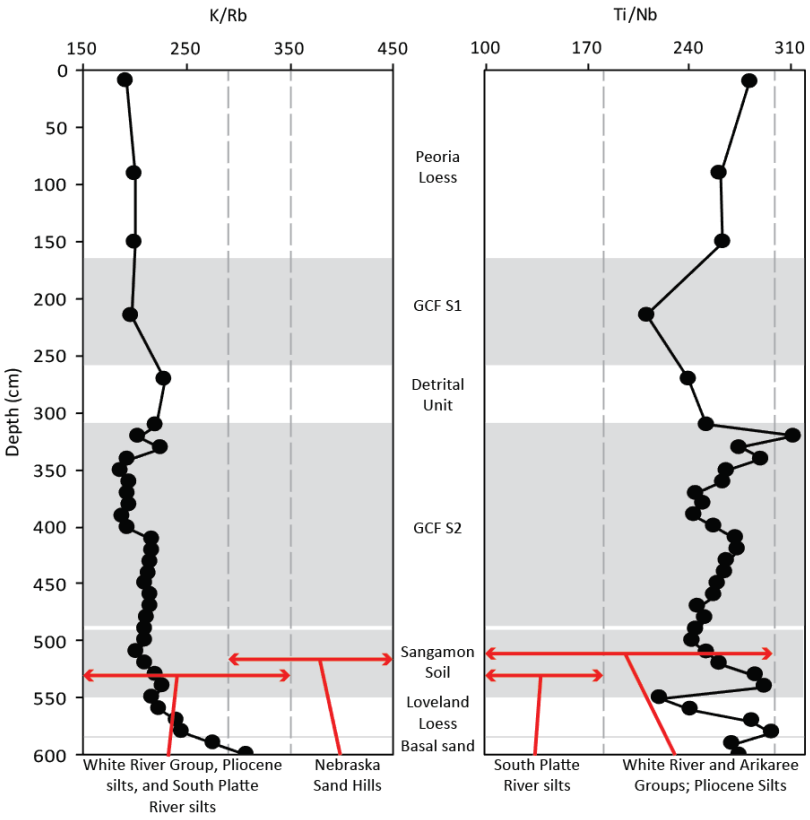

Figure 11. K/Rb and Ti/Nb ratios derived from core samples plotted with depth and stratigraphic units. Gray-shaded zones indicate soils. Provenance ranges and ratios modeled after Muhs et al. (2008).

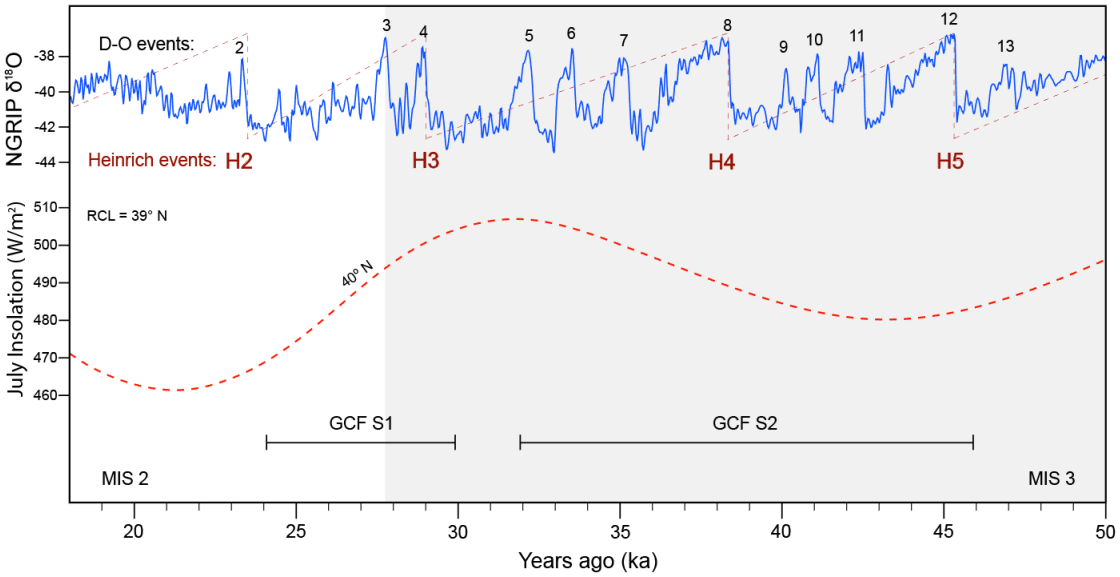

Figure 12. Correlations of $\delta^{18}O$ from NGRIP (Stuiver and Grootes, 2000) with numbered Dansgaard-Oeschger events (Bond et al., 1993), Heinrich events (Heinrich, 1988), July insolation curve from 40˚N latitude (Berger and Loutre, 1991), and periods of Gilman Canyon Formation soil development from MIS 3 (gray shading) through early MIS 2 (in white) dating 50 ka to 18 ka. Russell County Landfill located at ~ 39˚N latitude.